

POWER CONVERSION EFFICIENCY ENHANCEMENT OF ORGANIC SOLAR CELLS BY
ADDITION OF GOLD NANOPARTICLES

A THESIS SUBMITTED TO
THE GRADUATE SCHOOL OF NATURAL AND APPLIED SCIENCES
OF
MIDDLE EAST TECHNICAL UNIVERSITY

BY

DUYGU KOZANOĞLU

IN PARTIAL FULLFILLMENT OF THE REQUIREMENTS
FOR
THE DEGREE OF MASTER OF SCIENCE
IN
MICRO AND NANOTECHNOLOGY

SEPTEMBER 2012

Approval of the thesis:

**POWER CONVERSION EFFICIENCY ENHANCEMENT OF ORGANIC SOLAR CELLS BY
ADDITION OF GOLD NANOPARTICLES**

submitted by **DUYGU KOZANOĞLU** in partial fulfillment of the requirements for the degree of **Master of Science in Micro and Nanotechnology Department, Middle East Technical University** by,

Prof. Dr. Canan Özgen
Dean, Graduate School of **Natural and Applied Sciences**

Prof. Dr. Mürvet Volkan
Head of Department, **Micro and Nanotechnology**

Assist. Prof. Dr. Emren Nalbant Esenturk
Supervisor, **Chemistry Department, METU**

Examining Committee Members:

Assoc. Prof. Dr. Ayşen Yılmaz
Chemistry Department, METU

Assist. Prof. Dr. Emren Nalbant Esenturk
Chemistry Department, METU

Prof. Dr. Raşit Turan
Physics Department, METU

Assoc. Prof. Dr. Ali Çırpan
Chemistry Department, METU

Assist. Prof. Dr. Salih Özçubukcu
Chemistry Department, METU

Date: 13.09.2012

I hereby declare that all information in this document has been obtained and presented in accordance with academic rules and ethical conduct. I also declare that as required by these rules and conduct, I have fully cited and referenced all material and results that are not original to this work.

Name, Last name : Duygu KOZANOĞLU

Signature : _____

ABSTRACT

POWER CONVERSION EFFICIENCY ENHANCEMENT OF ORGANIC SOLAR CELLS BY ADDITION OF GOLD NANOPARTICLES

KOZANOĞLU, Duygu

M. Sc., Micro and Nanotechnology Department

Supervisor: Assist. Prof. Emren Nalbant ESENTÜRK

Co-Advisor: Prof. Dr. Raşit TURAN

September 2012, 66 pages

In the first part of the study, power conversion efficiency enhancement of organic solar cells by addition of gold nanorods and gold nanostars into PEDOT: PSS (Poly(3,4-ethylenedioxythiophene) poly(styrenesulfonate)) layer was investigated. Efficiency of each sample set has been characterized by measuring current density-voltage characteristics. The best efficiencies obtained during this study are 2.88 % and 2.54 % by addition of gold nanostars and nanorods, respectively. The increase in PCEs is notable when these values are compared with the ones (1.67 %) obtained with a reference device which is prepared without adding any gold nanoparticles under the same conditions.

In the second part of the study, branched gold nanoparticles were successfully grown directly on different types of surfaces such as glass, silicon wafer, and indium-tin-oxide (ITO) coated glass with a simple solution-based method in order to utilize them for further applications.

Keywords: organic photovoltaics, gold nanoparticles.

ÖZ

ALTIN NANOPARÇACIKLARIN EKLENMESİ İLE ORGANİK GÜNEŞ PİLLERİNİN VERİMLERİNİN ARTIRILMASI

KOZANOĞLU, Duygu

Yüksek Lisans, Mikro ve Nanoteknoloji Bölümü

Tez Yöneticisi: Yrd. Doç. Dr. Emren Nalbant ESENTÜRK

Ortak Tez Yöneticisi: Prof. Dr. Raşit TURAN

Eylül 2012, 66 sayfa

Çalışmanın ilk kısmında, organik güneş pillerinin PEDOT:PSS tabakasına altın nano çubuklar ve altın nano yıldızlar eklenerek, verimlerinin artırılması sağlanmaya çalışıldı. Her bir örnek setinin verimi akım yoğunluğu-voltaj karakteristiklerinden ölçüldü. Çalışma boyunca elde edilen en iyi verimler altın nano yıldızlar ve nano çubuklar için sırasıyla % 2.88 ve % 2.54 oldu. Aynı koşullar altında altın nanoparçacık eklenmeden üretilen referans cihazda elde edilen değerlerle (% 1.67) karşılaştırıldığında verimdeki artışlar dikkate değerdir.

Çalışmanın ikinci kısmında, daha sonraki uygulamalarda kullanılmak üzere basit bir solüsyon bazlı metot kullanarak, dallanmış altın nanoparçacıkların cam, indium-tin-oxide (ITO) kaplı cam ve Silikon levha gibi çeşitli yüzeyler üzerinde doğrudan büyütülmesi üzerine çalıştık.

Anahtar kelimeler: organik fotovoltaikler, altın nanoparçacıklar.

To My Family...

ACKNOWLEDGEMENTS

First, I would like to thank my advisor Assist. Prof. Dr. Emren NALBANT ESENTURK for her support and guidance throughout the whole time I have worked on my thesis. I also would like to thank Prof. Dr. Rařit Turan, Assoc. Prof. Dr. Ali irpan and Prof. Dr. Levent Toppare for giving me the opportunity work at GÜNAM.

I owe my deepest gratitude to Dođukan Hazar Apaydın for his contribution to this work.

I also would like to thank my lab-mates and friends Elin Dertli, Zhanar Sholanbayeva, Asude etin, Esra Öđün, ađla Arca, and Doruk Ergömen for their support, patience and kindness.

Finally, I would thank my family and my fiance Gülühan Kuzyaka for their patience, great understanding and moral support along my studies.

TABLE OF CONTENTS

ABSTRACT	iv
ÖZ	v
ACKNOWLEDGEMENTS	vii
TABLE OF CONTENTS.....	viii
LIST OF TABLES	x
LIST OF FIGURES	xi
CHAPTERS	
1. INTRODUCTION	1
2. NANOTECHNOLOGY AND GENERAL INFORMATION ABOUT NANOPARTICLES	4
2.1. INTRODUCTION	4
2.2. NANOSTRUCTURED MATERIALS.....	5
2.3. SYNTHESIS OF NANOSTRUCTURED MATERIALS	6
2.3.1. Top-Down Synthesis of Nanostructured Materials	6
2.3.2. Bottom-Up Synthesis of Nanostructured Materials.....	6
2.4. PROPERTIES OF NANOSTRUCTURED MATERIALS	7
2.5. METAL NANOPARTICLES.....	12
3. CONJUGATED POLYMER-BASED ORGANIC SOLAR CELLS.....	14
3.1. HUMAN ENERGY CONSUMPTION	14
3.2. RENEWABLE ENERGY SOURCES.....	15
3.3. ENERGY AND THE SUN	17
3.4. SOLAR ENERGY	18
3.5. SOLAR CELLS: HISTORY AND INTRODUCTION	19
3.6. NANOSTRUCTURED MATERIALS FOR SOLAR CELLS	22
3.7. ORGANIC SOLAR CELL MATERIALS	23
3.8. PREPARATION TECHNIQUES.....	26
3.9. OPERATING PRINCIPLES	29
3.10. ORGANIC PHOTOVOLTAIC DEVICE ARCHITECTURES.....	31
3.10.1. Bilayer Devices.....	32
3.10.2. Bulk Heterojunction (BHJ) Devices	33

3.11. EXCITONS.....	35
3.11.1 Exciton Formation.....	35
3.11.2. Exciton Diffusion	35
3.11.3. Exciton Dissociation	35
3.12. CHARACTERIZATION OF A SOLAR CELL DEVICE.....	36
3.12.1. Open Circuit Voltage.....	37
3.12.2. Short Circuit Current.....	38
3.12.3. Fill Factor.....	38
4. PHOTOVOLTAIC DEVICE PREPARATION BY ADDING GOLD NANOPARTICLES	39
4.1. INTRODUCTION	39
4.2. EXPERIMENTAL DETAILS.....	41
4.2.1. Preparation of Gold Nanoparticles.....	41
4.2.2. Photovoltaic Device Preparation	42
4.3. CHARACTERIZATION	44
4.4. RESULTS AND DISCUSSION	44
4.5. CONCLUSION	53
5. GROWTH OF BRANCHED GOLD NANOPARTICLES ON SURFACES.....	54
5.1. INTRODUCTION	54
5.2. EXPERIMENTAL SECTION	55
5.2.1. Materials.....	55
5.2.2. Preparation of Gold Seeds.....	55
5.2.3. Preparation of Branched Gold Nanostars.....	56
5.3. RESULTS AND DISCUSSION	57
5.4. CONCLUSION	62
REFERENCES	63

LIST OF TABLES

TABLES

Table 3.1. The use of fossil fuel compared with the reserves in 2004. (1 TW = 1 Terawatt= 10^{12} Watt, 1 ZJ = 1 zettajoule= 10^{21} J) [1].....	14
Table 3.2. The current use of various renewable energy sources as electricity and heating. (1 GW= 10^9 Js ⁻¹) [1].	15
Table 3.3. The current and targeted prices of renewable energy sources [Source: U. S. Department of Energy].....	16
Table 4.1. Photovoltaic parameters of organic solar cells incorporated in different concentrations of gold nanorods and gold nanostars (FF: Fill factor, J_{sc} : current density, V_{oc} : open circuit voltage, and PCE: power conversion efficiency).	49

LIST OF FIGURES

FIGURES

Figure 2.1. (a) Crystallization from the glass, (b) synthesis of a nanocrystalline material.	7
Figure 2.2. (a) Synthesis of nanomaterials by atoms having identical, chemical compositions by collecting of nm-sized crystals, (b) synthesis of nanomaterials by coating of atoms with different chemical properties than that of core atoms, (c) synthesis of nanomaterials by nm-sized crystals with different chemical compositions forming nanocomposites [21].	8
Figure 2.3. Size dependence of the optical absorption wavelength for gold nanoparticles [17].	9
Figure 2.4. The comparison of fashions of polycrystalline and nanocrystalline TiO ₂ into which a diamond pyramid penetrates [21].	10
Figure 2.5. (a) The sample has a total magnetization of zero, (b) The alignment of the domains by an external magnetic field. The total magnetization is not zero [27].	11
Figure 2.6: Transmission electron micrographs (top), optical spectra (left), and photographs of (right) aqueous solutions of gold nanorods of various aspect ratios. (a) aspect ratio 1,35±0,32, (b) aspect ratio 1,95±0,34, (c) aspect ratio 3,06±0,28, (d) aspect ratio 3,50±0,29, (e) aspect ratio 4,42±0,23 [30].	13
Figure 3.1. The world's present sources of energy [33].	15
Figure 3.2 Different sources of energy [33].	16
Figure 3.3. An illustration of the solar spectrum in space just outside the atmosphere (AM is negligible, AM 0) and the solar spectrum at the surface of the earth at the northern latitudes of Europe (AM 1.5) [1].	18
Figure 3 4. Illustration of the air masses of AM 0, AM 1.0 and AM 1.5 [1].	18
Figure 3.5. (a) Schematical drawing of energy bands and charge carriers of n-type and p-type semiconductors, (b) Schematical drawing of p-n junction [37].	20
Figure 3.6. The best research-cell efficiencies of various PV Technologies. (This graph was created and prepared by the National Renewable Energy Laboratory (NREL) for the US Department of Energy.) [2].	21

Figure 3.7. Chemical structures of the most commonly used conjugated organic polymers [1].	23
Figure 3.8. Examples of donor and acceptor materials used in polymer-fullerene bulk heterojunction (BHJ) solar cells [34].	24
Figure 3.9. Illustration of the photoinduced charge transfer. Electrons are excited in the PPV (polyvinylpyrrolidone) polymer and transferred to the C ₆₀ [49].	25
Figure 3.10. Chemical structures of PEDOT and PSS [1].	26
Figure 3.11. Schematic device structure for polymer/fullerene bulk heterojunction solar cells (top right). The active layer is sandwiched between two contacts: an indium-tin-oxide electrode coated with a hole transport layer PEDOT: PSS and a aluminum top electrode. Chemical structure of PEDOT: PSS (top left) [49].	28
Figure 3.12. Architectures of organic photovoltaic cell. (a) Bilayer cell, (b) Bulk heterojunction cell [51].	31
Figure 3.13. Bilayer configuration in organic solar cells [49].	32
Figure 3.14. Bulk heterojunction configuration in organic solar cells [49].	33
Figure 3.15. (a) Typical architecture of a single-junction polymer solar cell; (b) Current-voltage curve under illumination; (c) Energy levels diagram. The photovoltaic parameters extracted from the current-voltage curve; short-circuit current (I _{sc}); open-circuit voltage (V _{oc}); maximum output power (P _{max}) [52].	34
Figure 3.16. Structure of the photoactive layer (dark grey, donor; light grey, acceptor; white, anode; black, cathode). (a) bilayer heterojunction; (b) diffused bilayer heterojunction; (c) bulk heterojunction [52].	34
Figure 3.17. Current-voltage (I-V) curves of an organic solar cell. Almost no current flows in the dark [53].	36
Figure 4.1. (a) Schematic draw of a photovoltaic device, (b) Molecular structures of photovoltaic materials (P3HT: donor; PC ₇₀ BM: acceptor).	43
Figure 4.2. TEM images (A-D) of synthesized gold nanorods.	45
Figure 4.3. SEM images of synthesized gold nanostars.	45
Figure 4.4. UV-Vis absorption spectrum of the synthesized gold nanorods in water.	46
Figure 4.5. UV-Vis absorption spectrum of the synthesized gold nanostars in water.	46
Figure 4.6. Organic solar cell characteristics based on the volume percentage of nanorods in the PEDOT:PSS layer measured under illumination. The best efficiency	

and the highest current value were observed when 10 vol % of gold nanorod added to the solution.....	47
Figure 4.7. Organic solar cell characteristics based on the volume percentage of nanostars in the PEDOT:PSS layer measured under illumination. The best efficiency and the highest current value were observed when added 3 vol % of gold nanostar solution.....	48
Figure 4.8. IPCE vs. wavelength (spectral response) of devices produced by adding gold nanorods and gold nanostars into PEDOT:PSS layer. Inset shows closer look at the region between 650 nm and 1000 nm indicating higher IPCE obtained with gold nanostars compared to nanorods.....	51
Figure 5.1: Schematic diagram of the growth process of branched gold nanoparticles on surface.....	56
Figure 5.2. SEM images of seed particles attached on ITO surface.....	59
Figure 5.3. SEM images of the branched gold nanoparticles on ITO surface. ITO substrates were immersed in seed solution for 30 minutes. Figures from (a) to (d) show images at different magnifications.....	59
Figure 5.4. SEM images of the branched gold nanoparticles on glass surface. Glass substrates were immersed in seed solution for 30 minutes. Figure from A to D shows images at different magnifications.	60
Figure 5.5. SEM images of the branched gold nanoparticles on Si surface. Glass substrates were immersed in seed solution for 30 minutes. Figures from (a) to (d) show images at different magnifications.....	61

CHAPTER 1

INTRODUCTION

Most of the energy consumed by humans is derived from fossil fuels that are causing an environmental problem such as pollution. This consumption is increasing mostly due to the growth in human population or continuous industrialization of developing countries. Nonrenewable energy sources are limited and will not be sufficient in the near future. Therefore, the use of renewable energy sources should be improved. Solar energy is one of the most promising renewable energy source. The energy received from the sun by the side of the earth is approximately 1.2×10^5 TW, approximately 10000 times the energy consumed by humans in 2004 [1]. Photovoltaic technology is an attractive way of converting sunlight into electricity and can be a solution for the energy problem [2, 3]. Inorganic semiconductor-based photovoltaics are most commonly used solar cell devices [3]. For instance, silicon solar cells have long term stability and power conversion efficiencies about % 25 [2]. However, elevated temperature, high vacuum, and numerous lithographic steps are needed for production of these devices. All these increase the production cost and the payback may take several years [2].

The quest for developing efficient and affordable photovoltaic devices led to evolution of these devices with use of different materials instead of Si. Therefore, polymer based organic photovoltaics as a more affordable and convenient alternative to Si have attracted much interest and become subject of intense research. The organic, polymer-based photovoltaic devices provide the possibility of low production cost, room temperature processing, and mechanical flexibility [1-4]. Nonetheless, power conversion efficiency of polymer based organic solar cell is low

due to the high resistance of current organic semiconductors and low capability for photocarrier generation [1]. The power conversion efficiencies (PCEs) of organic solar cells are needed to be enhanced. In order to increase the PCE of organic solar cell, sufficient photocurrent and built-in potential should be created [5]. In addition, the photogenerated carriers should diffuse to donor and acceptor interfaces to be separated free charges. Since excitons, which are electron-hole pairs attracted to each other by the electrostatic coulomb force, are neutral, diffusion is not affected by any electric field but via random motions driven by the drift of concentration. Exciton diffusion lengths are around 10-20 nm for most conjugated polymers, and then recombination takes place. Excitons that recombine do not make a contribution to the photocurrent [2]. Sweep-out of the photogenerated carriers by the built-in potential competes with recombination of the photogenerated carriers within the bulk heterojunction film because of the low charge carrier mobility of the active materials. One solution might be reducing the recombination rate along with decreasing the film thickness to increase the device efficiency [3].

Noble metal nanoparticles can be used in solar cells to increase the efficiency of the device. They can achieve this both by transforming sunlight energy through the surface plasmon effect and/or by trapping the light in the film for longer path length [3]. Free electron in the conduction band of the metal atom is giving unique and significant optical properties. When light is absorbed by the nanoparticle, free electrons oscillate coherently through the electric field of the light wave. This is known as surface plasmon resonance and denoted strongly by noble metals [6, 7]. Surface plasmon resonance is the reason to observe the strong absorption band in the visible range [8, 9]. Gold nanoparticles with anisotropic morphologies are particularly interesting due to their unique optical and plasmonic properties, strong absorption in the near-IR [10-13]. Also, relatively large nanoparticles with diameters more than 10 nm can reflect and scatter light thus may increase the optical path length within the bulk heterojunction film [3]. This may enhance photogeneration of mobile carriers. Photovoltaic devices based on nanostructured composites of

electron donor and acceptor materials promise to deliver future solutions to the low-cost energy generation [3].

Nanoparticles with their unique catalytic, electronic, optical properties serve numerous ways of utilizing them in nanotechnology. Most applications require stabilization of nanoparticles on surfaces where they will be used. This can be done either by transferring nanoparticles to a surface after they were synthesized in either liquid or gas phase. Another route might be growing nanoparticles directly on surfaces such as Si, ITO or glass. This approach provide practical way of stabilizing nanoparticles on surfaces and employing their best properties for various applications including photovoltaic devices [14].

CHAPTER 2

NANOTECHNOLOGY AND GENERAL INFORMATION ABOUT NANOPARTICLES

2.1. INTRODUCTION

Richard P. Feynman's talk in 1959 which is titled "There's Plenty of Room at the Bottom" is assumed as the starting point of the idea of nanotechnology. The things on a small scale could be controlled and manipulated was the matter of his talk. Progress of nanotechnology since 1980 has indicated his envision [15].

A nanometer is described as a distance of one-billionth of a meter [16]. Materials with at least one characteristic dimension in the range of nanoscale are nanostructured materials. Nanostructured materials have unique and interesting behaviour. When the size of the material reduces to the range of 1 to 100 nm, different properties are attributed to the material. This provides new technological opportunities [17]. Controlling and manipulating the chemical and physical properties of nanostructured materials and preparing them for specific applications are possible via the advances in nanoscience [18, 19]. The fabrication of physical, chemical, and biological systems at nanoscale and adjustment them to larger systems are subjects of nanotechnology [15, 17]. Molecular and atomic dimensions take an important part instead of classical physical principles in nanotechnology [20].

Development of new technologies requires miniaturization of devices in nanoscale. For instance, for computer technology invention of integrated circuits requires the increase of the number of transistors. Nanotechnology provide us to increase data

density but reduce the dimensions of devices. It is obvious that the probable consequences of nanotechnology for society will be significant [19]. Nanoelectronics, medicine, energy, biotechnology, information technology, and national security are various areas that would make progress through nanotechnology [15].

2.2. NANOSTRUCTURED MATERIALS

Materials having a characteristic length scale on the order of a few nanometers are defined as nanostructured materials [21]. In other words nanomaterials are structures having one dimension below 100 nm and a second dimension below 1 μm [20]. The properties of nanostructured materials vary as the size is getting reduced and the shape is altered [21]. Hence, the importance of controlling the size and shape of the materials on the atomic level has been increased as an interdisciplinary field [21]. When compared to the properties of nano-sized particles and larger particles of the same specimen, it is obvious that their physical and chemical properties are rather different. While properties of larger particles are controlled by physical laws, the ones of nano-sized particles are controlled by quantum mechanics. For instance, electrical conductivity, color, solubility, magnetization, strength can be counted as changing properties [22]. These changes also affect quantum confinement in semiconductor particles, surface plasmon resonance in some metal particles, and superparamagnetism in magnetic materials [18]. Another example, while electrons flow in streams at the macro scale, wave-like properties of electrons result the electron flow in insulators as the size is decreasing to the nanoscale [16].

Surface properties of a solid material are very different from the ones of the bulk. The number of surface atoms is small as compared to the number of bulk particles for solid material, but the number of surface atoms is more than the number of bulk particles for nanostructured material. The changes in the properties of surface atoms and molecules are connected to the states of molecules on surfaces or

interfaces [20]. Nanoparticles have very large surface area where reactions occur resulting reactions to happen faster [16]. Nanoparticles are surface reactive and interfacial chemical interactions affect their behaviour. Therefore, the atoms of nanomaterials placed at interfaces behave differently [18].

2.3. SYNTHESIS OF NANOSTRUCTURED MATERIALS

2.3.1. Top-Down Synthesis of Nanostructured Materials

This method is downsizing the bulk particles and joining them together in a specific fashion [17, 23, 24]. Bulk material is splitted up or miniaturized to obtain the likely structure having desired properties [17]. High-energy milling, chemical processing, electro-explosion, laser ablation, sputtering, and vapor condensation are examples of top-down synthesis method [23].

2.3.2. Bottom-Up Synthesis of Nanostructured Materials

Bottom-up synthesis techniques are based on production of nanostructures by using atoms, molecules, and nanoparticles as the building blocks [17, 23]. Precipitation, sol-gel methods, chemical vapor deposition, and self-assembly routes are some examples of bottom-up approach.

In order to produce nanocrystalline materials, two ways are used in bottom-up synthesis method; self-organization and self-assembly of the individual building blocks [17]. Bottom-up method starts with the nucleation of countless crystallites in the glass by annealing, composing a nanocrystalline material (Figure 2.1).

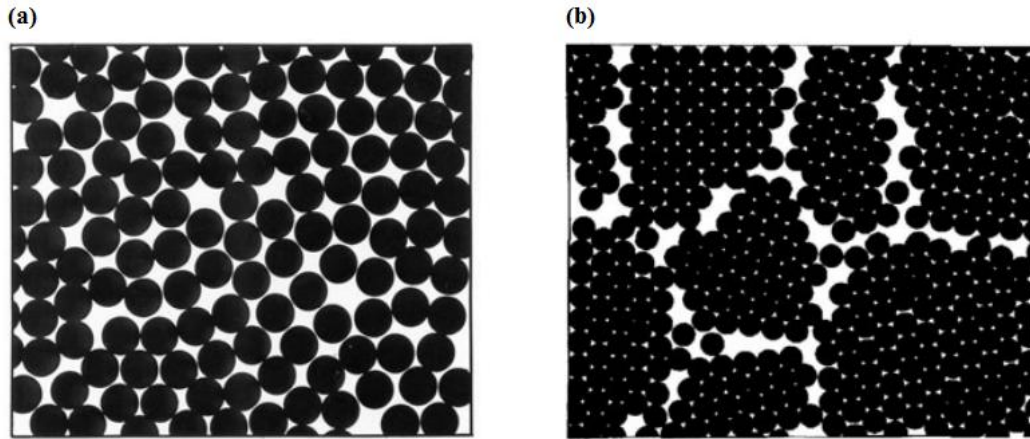


Figure 2.1. (a) Crystallization from the glass, (b) synthesis of a nanocrystalline material.

Low-cost mass production, exhibition of materials having a little or no porosity may be counted as the advantages of this method but crystals with different chemical compositions may not be produced via this method [21].

2.4. PROPERTIES OF NANOSTRUCTURED MATERIALS

The density, spatial distribution, and the strength of bonds between the particles control the properties of a material [20]. Size, atomic structure, and chemical composition also affects the properties of solids. Therefore, a solid and a single crystal exhibit different and unique properties (Figure 2.1) [21].

The number of atoms located at the surface increases as the size of particles decreases [16]. Correspondingly, many atoms of a nanoparticle is located at grain boundaries. Thus, reduced-dimensional systems exhibit very different properties as compared to their bulk counterparts [17]. The bonding and electronic structures of an atom positioned at the surface differs from the others [16, 17]. Their higher energy states give them the ability to react easily with neighboring particles [16]. Surface free energy, and interatomic spacings are also increase when the particle size decreases resulting the change in the thermal properties of materials. For instance, the melting point of gold nanoparticles decrease when their sizes are

reduced. In the range of size less than 10 nm this decrease occurs more sharply [25]. Furthermore, the bulk material needs more energy to remove an electron from the surface than corresponding small materials. When the size of the material changes, the ionization energy fluctuates resulting the change in the chemical reactivity. The change in the chemical reactivity of nanoscale particles may be result from very high surface area to volume ratios [17].

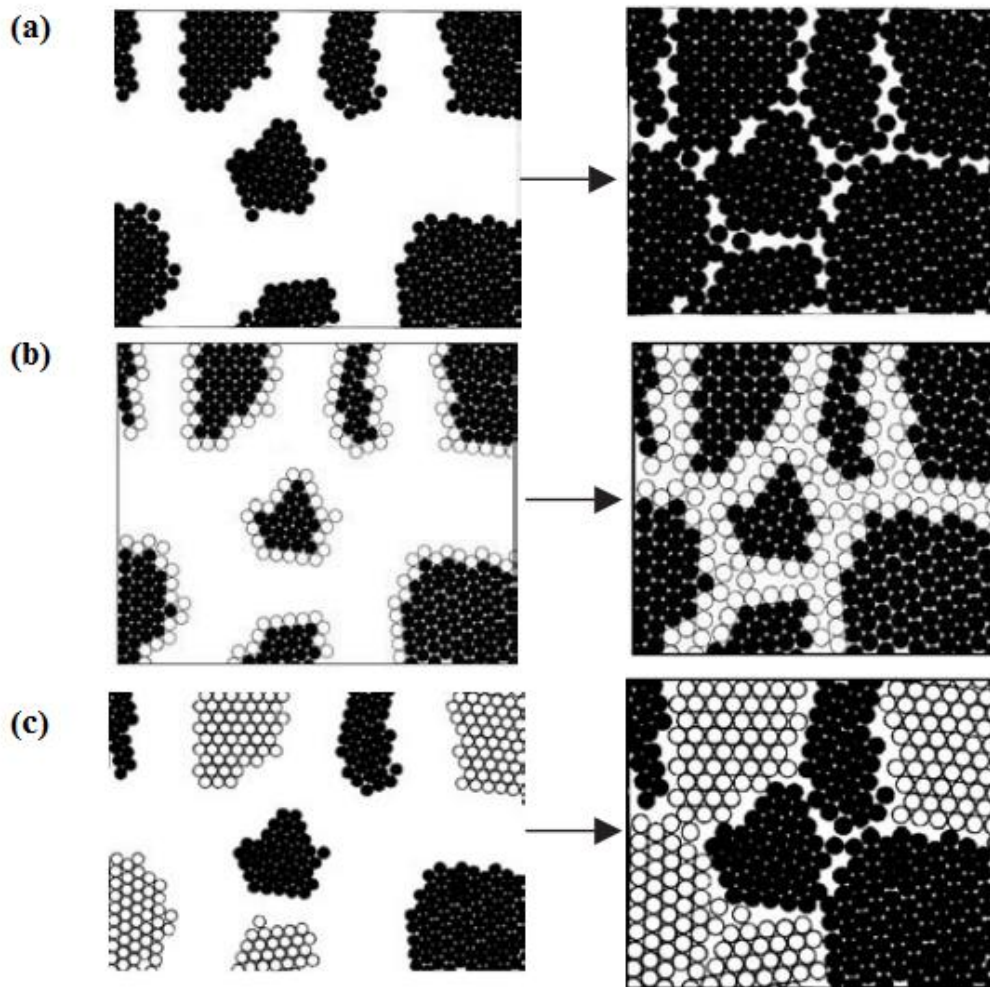


Figure 2.2. (a) Synthesis of nanomaterials by atoms having identical, chemical compositions by collecting of nm-sized crystals, (b) synthesis of nanomaterials by coating of atoms with different chemical properties than that of core atoms, (c) synthesis of nanomaterials by nm-sized crystals with different chemical compositions forming nanocomposites [21].

Quantum properties of nanocrystals result from band gaps that are dependent on size resulting color emission by nanocrystals. Nanocrystals exhibit quantum

properties when the dimensions of excitons are smaller than electron-hole distance. This results in the quantization of the state of free charge carriers within a nanocrystal. For instance, when the size of metallic system decreases, metal-insulator transitions may be undergone a change forming a forbidden energy band gap. The nature and separation of the energy levels change with the change of transport properties by the reduction of size [17, 26]. Reducing the size of the structure also affects the energies of the highest occupied molecular orbital (HOMO), as it is the valence band, and the lowest unoccupied molecular orbital (LUMO), as it is the conduction band. This results the changes in optical properties, such as colour. Figure 2.3 illustrates that different sizes of gold nanoparticles show different optical absorption spectra. The photocatalysis, photoconductivity, photoemission, and electroluminescence are also affected by reduced size [17].

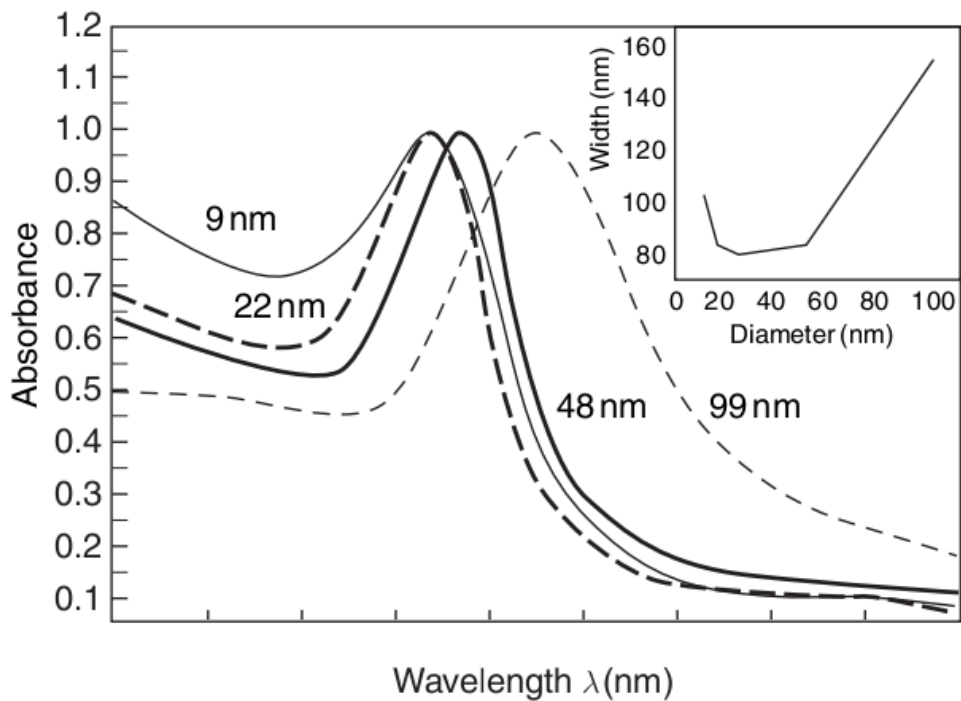


Figure 2.3. Size dependence of the optical absorption wavelength for gold nanoparticles [17].

The wave-like property of the electrons induces the changes in electronic properties as the size of the system decreases. If the size of the system approximate the de

Broglie wavelength, the discrete energy states are observed. For instance, when the size of the conducting materials decreases below a certain level, they become insulators because the energy bands no longer overlap. Electrons can tunnel quantum mechanically between two adjacent nanostructures through their wave-like nature. The transportation of electrons occurs by scattering with phonons, impurities or other carriers or by scattering at interfaces in macroscopic systems. Besides, electrons move randomly and are transported diffusively. As the size of the system becomes smaller, random transportation is dissipated and scattering centres are eliminated. Besides, transportation of electrons occur like throwing [17].

It is possible to control the properties of materials (for example mechanical and magnetic properties) by controlling the size and shape of materials [21]. Nanostructures have very different mechanical properties as compared to their bulk counterparts. For instance, their interface-driven processes such as plasticity, ductility, and strain to failure exhibit enhancements [17]. The mechanical properties are affected considerably by the number of grain boundaries in nanocrystalline materials (Figure 2.4). For instance, nanocrystalline materials elongate more as compared to bulk polycrystals having same chemical properties [21].

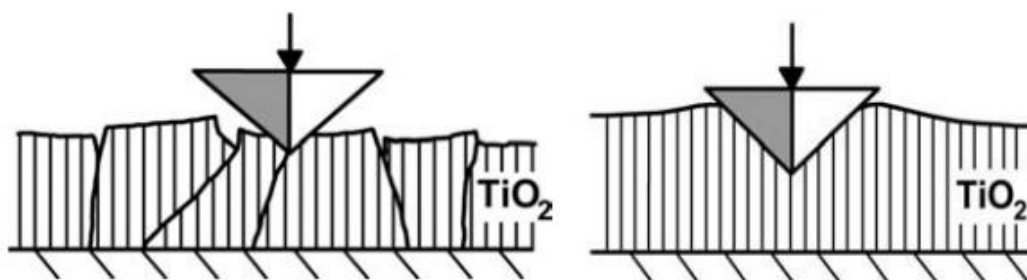


Figure 2.4. The comparison of fashions of polycrystalline and nanocrystalline TiO_2 into which a diamond pyramid penetrates [21].

Nanocrystalline materials are harder than a single crystal with the same chemical composition. Moreover, when the size reaches to 3 nm, the hardness of the nanocrystal becomes closer to the that of diamond [21].

Atoms of nanostructures couple magnetically with their neighbouring atoms [17]. Ferromagnets are materials with atoms having strong magnetic moments [27]. While small magnetic nanoparticles form only one magnetic domain and exhibit superparamagnetic property, bulk ferromagnetic materials form multiple magnetic domains [17]. The reason of the properties of ferromagnetic materials are both strong magnetic moments carried by their atoms and small regions composing the material called magnetic domains. While domains are magnetic, the bulk material may not exhibit magnetic property. Because the orientation of domains is random to each other (Figure 2.5) [27]. Thermal fluctuations cause the random distribution of the magnetization of the various particles [17]. If magnetic domains are aligned by an external magnetic field or by passing electric field through the material, the magnetization of ferromagnetic material occurs. Moreover, the magnetic field becomes stronger as the number of aligned domains increases. The magnetization of a material reaches a saturated point when there is no non-aligned domains left. After this, any additional external force can not cause an increase in the magnetization [27].

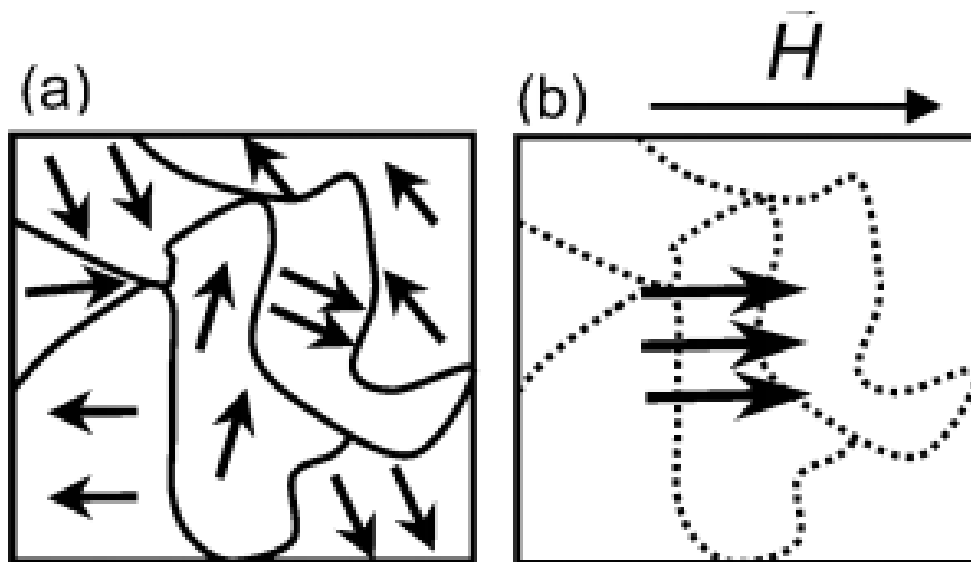


Figure 2.5. (a) The sample has a total magnetization of zero, (b) The alignment of the domains by an external magnetic field. The total magnetization is not zero [27].

The exchange and dipolar coupling between attached ferromagnetic grains are also possible for nanocrystals. Moreover, the grain size reduces to the fashion of ferromagnetic single domain [21].

2.5. METAL NANOPARTICLES

Unusual characteristics of metal nanoparticles upon their interaction with light were noticed at the early stages of modern civilization [28]. Michael Faraday investigated the red color of gold colloids and attributed this to the size of the particles [29]. In fact, gold is used for 5000 years. Indian used gold in medicine, Egyptians in dentistry in ancient years. Chinese people cooked their rice with a gold coin to renew their body. Romans used colloidal gold for glasses and vases to give them color [19]. Actually, they used very small amount of gold (about 40 parts per million). These particles were in the range of nanoscale [19]. In 1831, a deeper understanding of the physical mechanism was supplied by the pioneering study of Gustav Mie in 1908 [28]. He explained the colors of metal nanoparticles by explaining absorption and scattering of light by small spheres [29]. With the advent of technology, characterization devices such as SPM, TEM were developed resulting an understanding of the properties of nanostructured materials [19].

Metal particles in nanoscale are of great interest due to their unusual properties. The mean free path of an electron in a metal at room temperature is ~ 10 - 100 nm. It can be predictable that as the metallic particle becomes smaller to this dimension, unusual effects should be observed. For example, gold nanospheres of diameter ~ 100 nm or smaller appear red or gold nanoparticles of diameter less than ~ 3 nm are no longer unreactive but can catalyze chemical reactions [30].

Metallic nanoparticles may exhibit collective electron excitations (surface plasmons) when exposed to light. They can concentrate and manipulate light in a volume much less than the incident wavelength. The resonance energy for these enhancements depends on the size, shape, and proximity of the nanoscale objects.

Pairs of these particles can couple and enhance local electric fields by factors of 10^5 or more [31].

The optical properties of silver and gold nanoparticles are tunable throughout the visible and near-infrared region of the spectrum as a function of nanoparticles size, shape, aggregation state, and local environment (Figure 2.6). For nanorods and nanowires, the plasmon band of the metal is split into two: the longitudinal plasmon band and the transverse plasmon band. The longitudinal plasmon band, corresponding to light absorption and scattering along the long axis of the particle. The transverse plasmon band, corresponding to light absorption and scattering along the short axis of the particle [30].

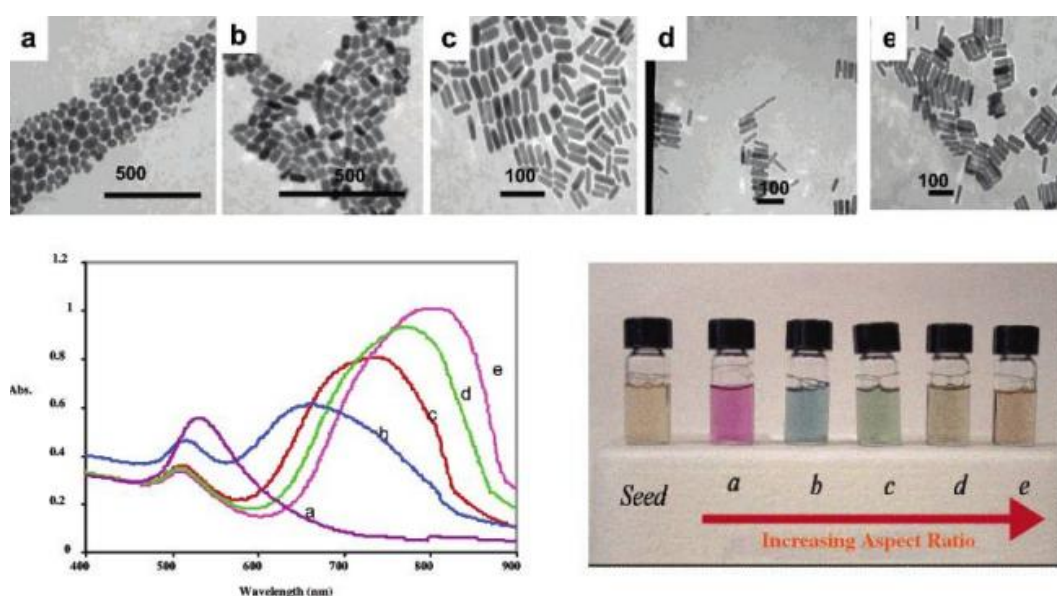


Figure 2.6: Transmission electron micrographs (top), optical spectra (left), and photographs of (right) aqueous solutions of gold nanorods of various aspect ratios. (a) aspect ratio $1,35 \pm 0,32$, (b) aspect ratio $1,95 \pm 0,34$, (c) aspect ratio $3,06 \pm 0,28$, (d) aspect ratio $3,50 \pm 0,29$, (e) aspect ratio $4,42 \pm 0,23$ [30].

CHAPTER 3

CONJUGATED POLYMER-BASED ORGANIC SOLAR CELLS

3.1. HUMAN ENERGY CONSUMPTION

Energy sources such as coal-derived fuel produces waste which is overhanging danger for environment and requires costly methods to charge them off [18, 32]. The human energy consumption in 2004 was approximately 15 terawatts in 2004. 87% of this consumption was occupied from fossil-fuel. The demand is increasing every day because of the reasons such as continuous industrialization of developing countries and growth in human population. The foreseeable level of energy consumption by humans is 28-35 terawatts by the year 2050 [1].

Table 3.1. The use of fossil fuel compared with the reserves in 2004. (1 TW = 1 Terawatt= 10^{12} Watt, 1 ZJ = 1 zettajoule= 10^{21} J) [1].

	Form	Consumption(TW)	Annual Consumption (ZJ year ⁻¹)	Energy reserve (ZJ ²)	Time left (years)
Coal	Solid	3.8	0.12	290	2400
Oil	Liquid	5.6	0.18	57	316
Natural gas	Gaseous	3.5	0.11	30	272

There are still plenty of fossil fuels, however, carbon dioxide and toxic waste are non-desirable results of fossil fuels. Overmuch abuse of energy occupied from fossil

fuels causes global warming, therefore renewable and non-CO₂-emissive sources should be found [1].

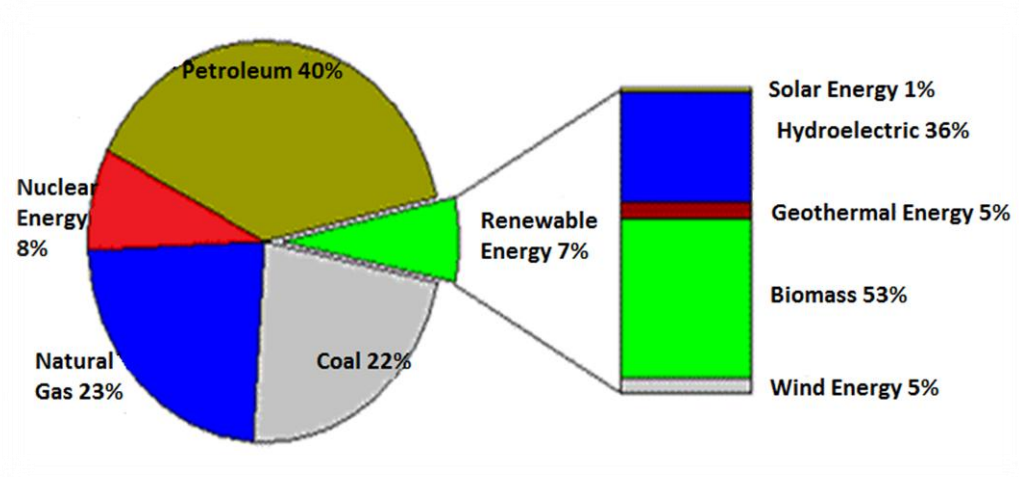


Figure 3.1. The world's present sources of energy [33].

3.2. RENEWABLE ENERGY SOURCES

There are a plenty of renewable energy sources such as solar energy, biomass energy, geothermal energy, wind energy, and hydropower [1].

Table 3.2. The current use of various renewable energy sources as electricity and heating. (1 GW=10⁹ Js⁻¹) [1].

	Electricity (GW)	Heating (GW)	Total (GW)
Solar energy	5.4	88	93.4
Biomass energy	44	220	264
Geothermal energy	9.3	28	37.3
Wind energy	59	–	59
Hydropower	816	–	816
Ocean energy	0.3	–	0.3
Total	934	336	1270

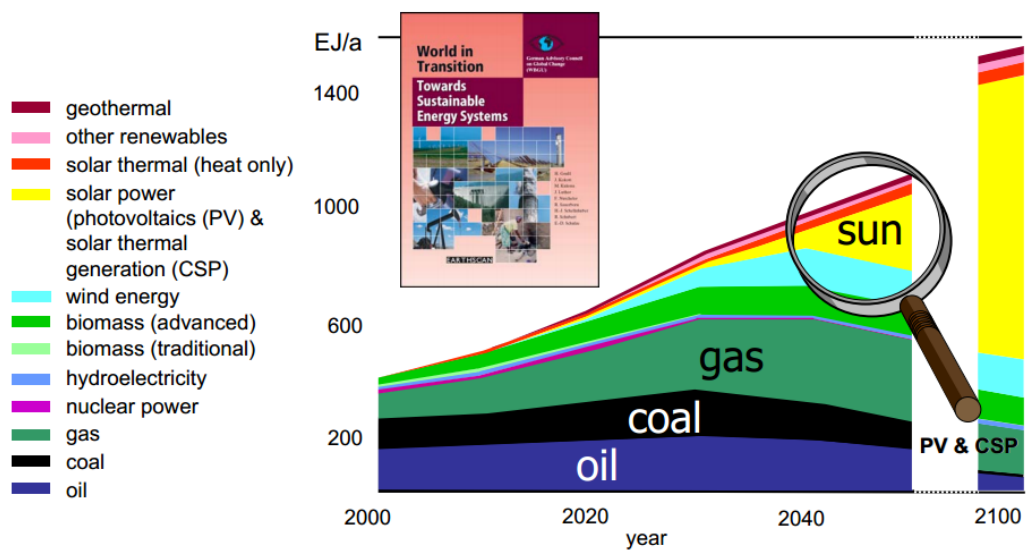


Figure 3.2 Different sources of energy [33].

China has targeted to derive 10 % of energy from renewable energy sources in 2010. The target set by the European Union (EU) is 12 % of energy and 22 % of electricity from renewable energy sources in 2010. In the United States, state governments are spending money on development of renewable technologies. The money spent raised from \$10 billion to \$89 billion in 2012 [18].

Table 3.3. The current and targeted prices of renewable energy sources [Source: U. S. Department of Energy].

Renewable Source	Approximate Price per kilowatt hour (1980)	Approximate Price per kilowatt hour (2003)	Approximate Price Target
Wind	\$ 0.80	\$ 0.05	\$ 0.03 (2012)
Solar (PV)	\$ 2.00	\$ 0.20-0.30	\$ 0.06 (2020)
Biomass	\$ 0.20	\$ 0.10	\$ 0.06 (2020)
Geothermal	\$ 0.15	\$ 0.05-0.08	\$ 0.04 (2010)

There are numerous challenges to be overcome to replace fossil fuels with renewable energy such as affordability and storage. Nanotechnology holds great promise to enhance renewable technology [18].

3.3. ENERGY AND THE SUN

The sun is positioned at the center of our solar system. It is composed of 70% hydrogen, 28% helium, and 2% of all the other elements. The diameter of sun is 1.39×10^7 m, and the mass of it is 1.989×10^{30} kg. The mass of the sun is 99.8% of the total mass of our solar system. The temperature is 15.6×10^6 K and pressure is more than 25×10^{10} atmosphere in the center of the sun. These values of the temperature and pressure makes nuclear fusion reactions, therefore producing energy possible. In the fusion process 7×10^{11} kg of hydrogen is converted into 695×10^9 kg of helium every second at the center of the sun. This process provide 5×10^9 kg of energy in the form of gamma rays, which is equal to 3.89×10^{26} J.

The distance between the sun and the earth is 149.6×10^8 m. The earth has a mass of 5.98×10^{24} m and a diameter of 12.756×10^3 m. The energy density becomes lower because energy from the sun is emitted in all directions. The spectrum of the sunlight changes while passing through the atmosphere. The energy is 1366 Wm^{-2} just outside the earth's atmosphere but some of the energy of visible light passing through the atmosphere is lost. The reason is that atmospheric gases absorb certain wavelength region, nonetheless the sunlight does not pass through any atmosphere but empty space in space just outside the atmosphere (Figure 3.3). The abbreviation AM is described as the spectrum obtained after passing through a certain air mass, in other words the amount of air mass that the sunlight has passed through. The equator is the closest place to the sun and light can travel the shortest distance. There the sun's spectrum is termed AM 1.0. The sunlight has to travel longer distances to reach the surface in northern Europe and the United States. There the air mass is termed AM 1.5 corresponding to a receiving surface tilted 37 degree toward the equator (Figure 3.4) [1].

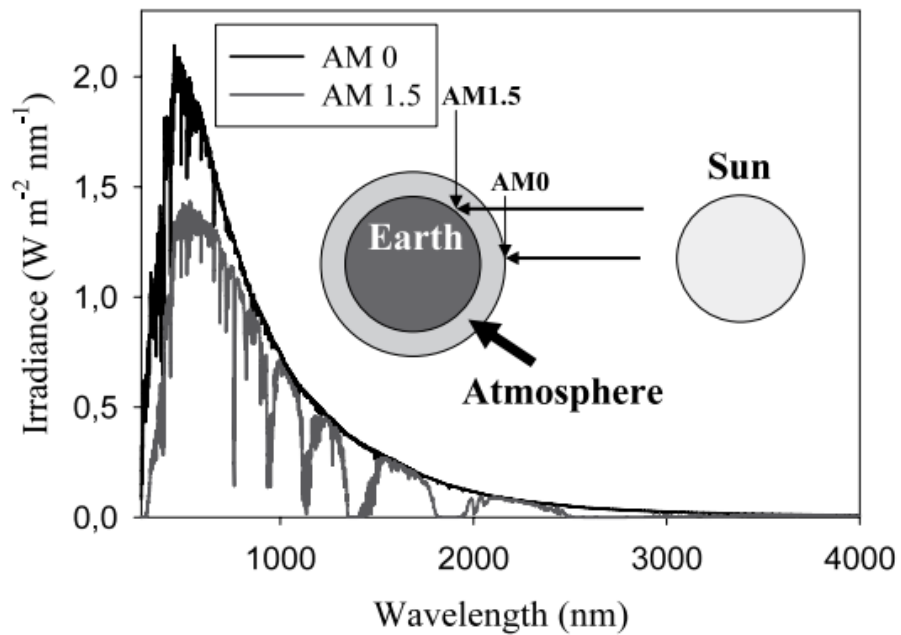


Figure 3.3. An illustration of the solar spectrum in space just outside the atmosphere (AM is negligible, AM 0) and the solar spectrum at the surface of the earth at the northern latitudes of Europe (AM 1.5) [1].

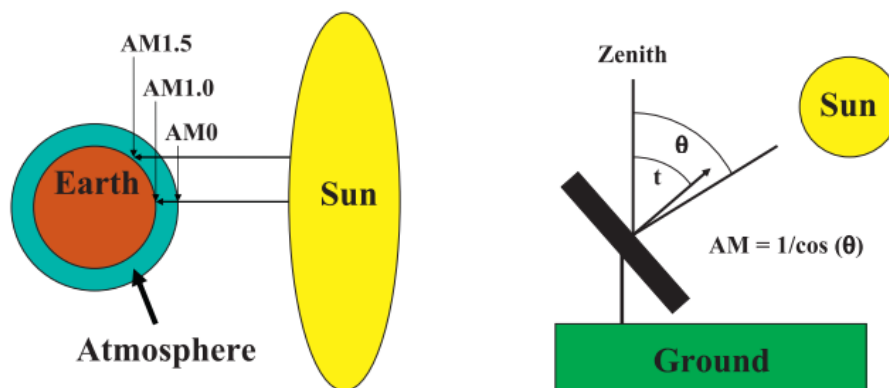


Figure 3 4. Illustration of the air masses of AM 0, AM 1.0 and AM 1.5 [1].

3.4. SOLAR ENERGY

The side of the earth that is exposed to the sun receives about 1.2×10^5 TW from the sun. This amount of energy is about 10000 times the energy that is consumed in 2004. This means that there is plenty of energy that can be obtained from the sun.

The energy coming from the sun can be converted by the energy extraction devices such as photovoltaic devices [1, 34]. There is some problems associated with solar energy because the energy that is received and converted into electricity is lost when it is not used as it is generated. The energy storage is a very important challenge if there is no need to use it immediately [1].

3.5. SOLAR CELLS: HISTORY AND INTRODUCTION

In 1839 French physicist Edmond Becquerel discovered the photovoltaic effect for the first time [32]. Solar cells are first used in the last half of 19th century. Researchers including William Grylls Adams and his student Richard Evans Day discovered the dependence of material performance on the amount of light falling of it. They discovered that light cause a solid material to produce electricity, which was something new. However, the science couldn't explain why selenium produced electricity. Scientists theorized that when light hits a material such as selenium, more powerful photons pack enough energy in order to knock the weakly bounded electrons from their orbits. Flowing liberated electrons produce electricity. Furthermore selenium solar cells were not produced because they could only half a percent of solar energy, so they were not enough to be a power source [35]. In 1954 the first crystalline silicon photovoltaic device was investigated at Bell Laboratories using a solid-state semiconductor junction. They could produce less than a watt of power. Today's solar panels can produce several hundred megawatts in year [32].

A solar cell is a large-area diode conducting a charge in only one direction [36]. In order to generate a conventional solar cell, an inorganic semiconductor doped to form a p-n junction is used. While excess of positive charges (holes) are covered by p-side, excess of negative charges (electrons) are covered by n-side (Figure 3.5). The formation of an electric field occurs in the region near the junction [32]. After the absorption of light by device, electron-hole pairs which have energy greater than band gap are generated. As the light intensity increases, the number of electron-hole pairs increases. Electron-hole pairs dissociate due to the electric field

generated by depletion region and accelerated to the corresponding electrodes [32, 37].

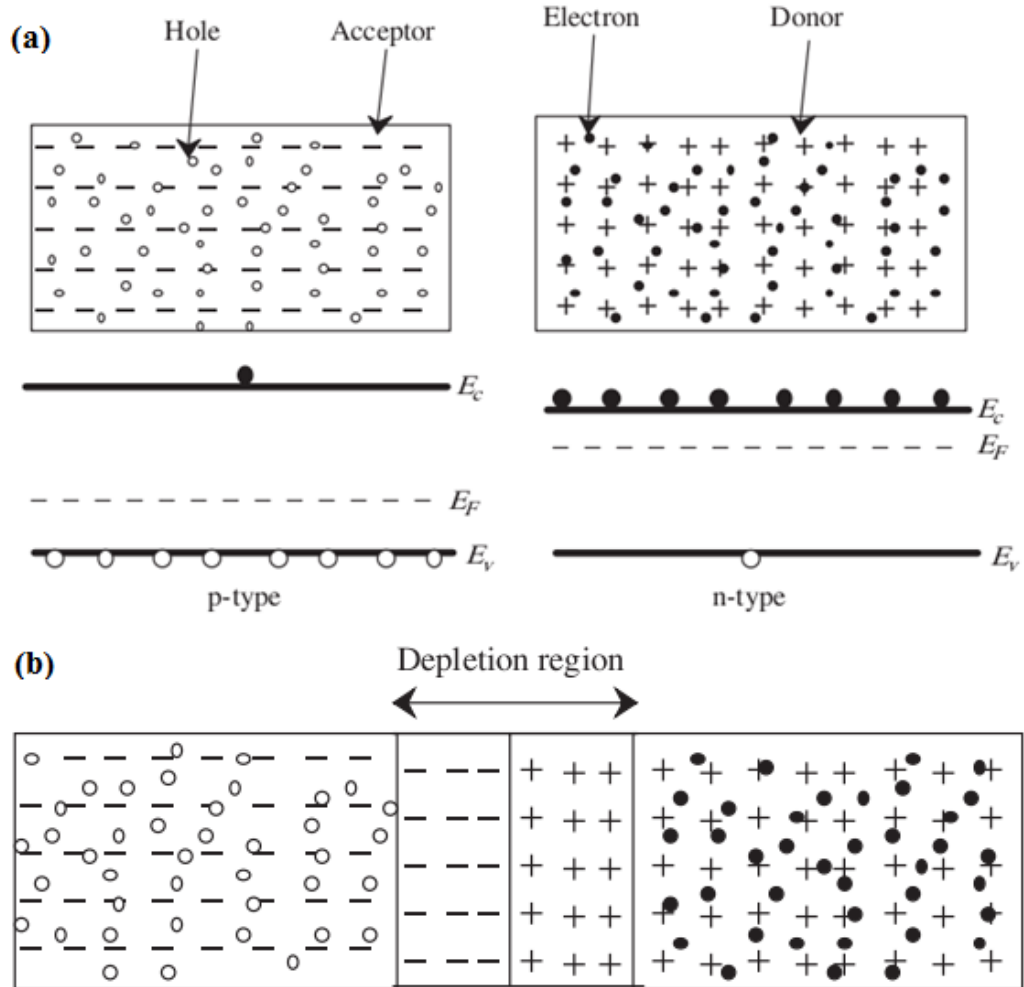


Figure 3.5. (a) Schematic drawing of energy bands and charge carriers of n-type and p-type semiconductors, (b) Schematic drawing of p-n junction [37].

First generation solar cells, crystalline silicon wafer based solar cells, form the majority of photovoltaic market. They have 25% power conversion efficiency (PCE) particularly. However, their fragility makes production steps difficult. Elevated temperature, high vacuum, and numerous lithographic steps are needed for the production of silicon wafer based solar cells. Moreover, the cost of high purity silicon wafers is very high and purchasing and installation costs may be regained in several years. Through the disadvantages of silicon wafer based solar cells, second generation solar cells-thin film solar cells were investigated. The production steps

are easier and their costs are lower as compared to first generation solar cells. Multijunction tandem cells, dye-sensitized solar cells (DSSCs), organic solar cells based on small molecules and conjugated polymers, and organic and inorganic hybrid solar cells are included in the group of third generation solar cells [2].

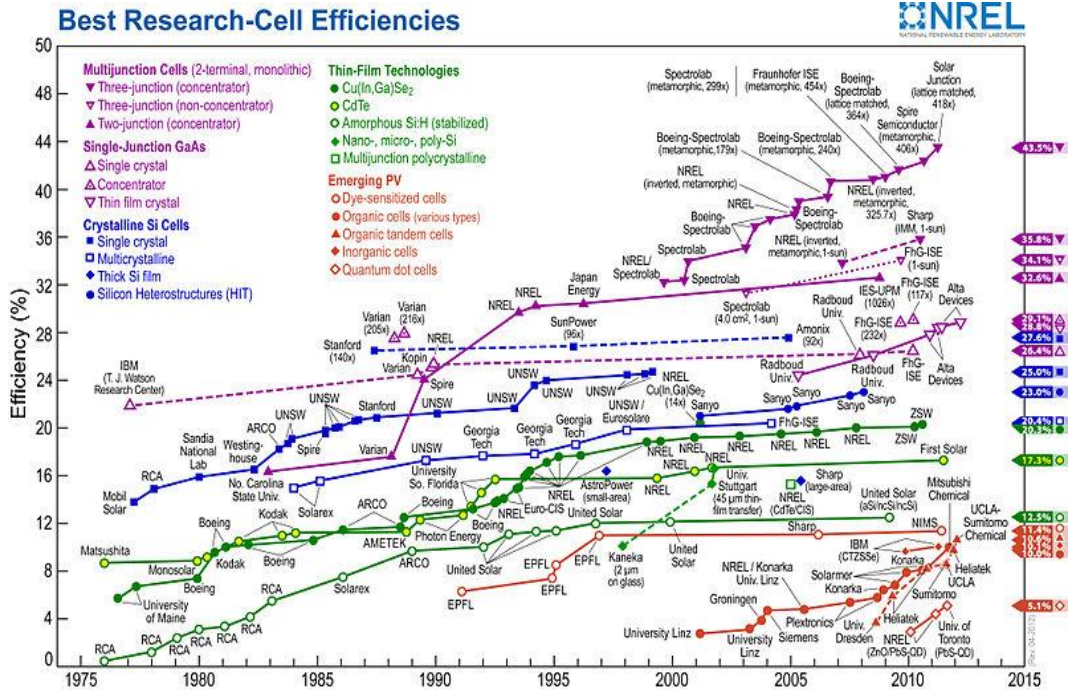


Figure 3.6. The best research-cell efficiencies of various PV Technologies. (This graph was created and prepared by the National Renewable Energy Laboratory (NREL) for the US Department of Energy.) [2].

Organic solar cells are promising for producing electricity from solar energy [2]. They have the advantages of low production cost, processing at room temperature, and mechanical flexibility [4]. However, low efficiency and stability are the problems of organic solar cells [32]. Nonetheless, the studies to enhance the PCEs of organic solar cells which was initiated by Tang et al. in 1986, reached a level above 7 % currently [38, 39].

An interpenetrating network of electron-donor and electron-acceptor components provides highly efficient exciton dissociation and high photocurrent. This type of solar cells are called as ‘bulk heterojunction type of organic solar cells’. They provide continuous charge transportation through the film [40]. The importance of

the bulk heterojunction type of solar cells is resulted from the creation of a large interfacial area between the donor and acceptor materials where charge separation occurs [1].

Excitons generated on excitation have short lifetime and their diffusion length is 5-20 nm. There are some very important factors such as the size of the individual domains and the connection of domains to make continuous transportation of both electrons and holes to the electrodes possible [1].

The efficiency can be increased by some adjusting fabrication parameters and some new methods such as embedding noble metal nanoparticles into buffer layer.

The progress of the best research-cell power conversion efficiencies based on various materials and technologies updated till June 2010 is summarized in Figure 3.6 [2].

3.6. NANOSTRUCTURED MATERIALS FOR SOLAR CELLS

In order to utilize the performance of solar cells, numerous studies have been reported recently [41]. There are studies about microcrystalline thin film solar cells consisting of nano-sized crystallites [37]. In order to enhance electron transportation and increase light trapping as well, nanoparticles (i.e. nanorods, nanowires, nanostars, nanospheres) can be used [3, 42-47].

Unique optical properties of nanostructured materials can be utilized in applications such as optoelectrical devices. Materials used to produce polymer based organic solar cells consisting of polymer nanostructured networks absorb strongly in the visible region. Besides, their size can be reduced into nanometer scale to reduce the bulk resistance. Doping organic photovoltaics with polymer-based inorganic nanoparticles or nanocrystals may be a solution to solve the problem of low electron mobility [34].

Excitons are generated after photon absorption by the polymer-based organic solar cell. Then, they separate into electron-hole pairs when they reach the junction. If the electron-hole pairs travel more than a few nanometer, the possibility of recombining of the electrons and holes increases. Thus, photo-induced charge separation is more efficient in the composite nanostructures [34].

3.7. ORGANIC SOLAR CELL MATERIALS

Conjugated polymers are used as active layer material in solar cells since they provide absorption of sunlight as well as creation and transportation of photogenerated charge carriers. The poly(phenylenevinylene)s (PPVs) such as poly[2-methoxy-5-(2-ethylhexyloxy)-1,4-phenylenevinylene] (MEH-PPV) and poly[2-methoxy-5-(3,7-dimethyloctyloxy)-1,4-phenylenevinylene] (MDMO-PPV) are most commonly used conjugated polymers (Figure 2.7) [1]. The devices produced with these polymers reached the efficiency of 2.5 % [1, 48].

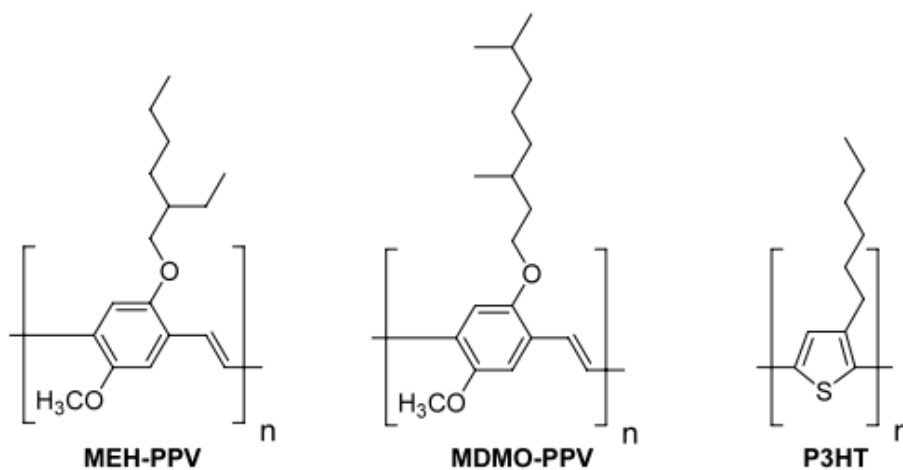


Figure 3.7. Chemical structures of the most commonly used conjugated organic polymers [1].

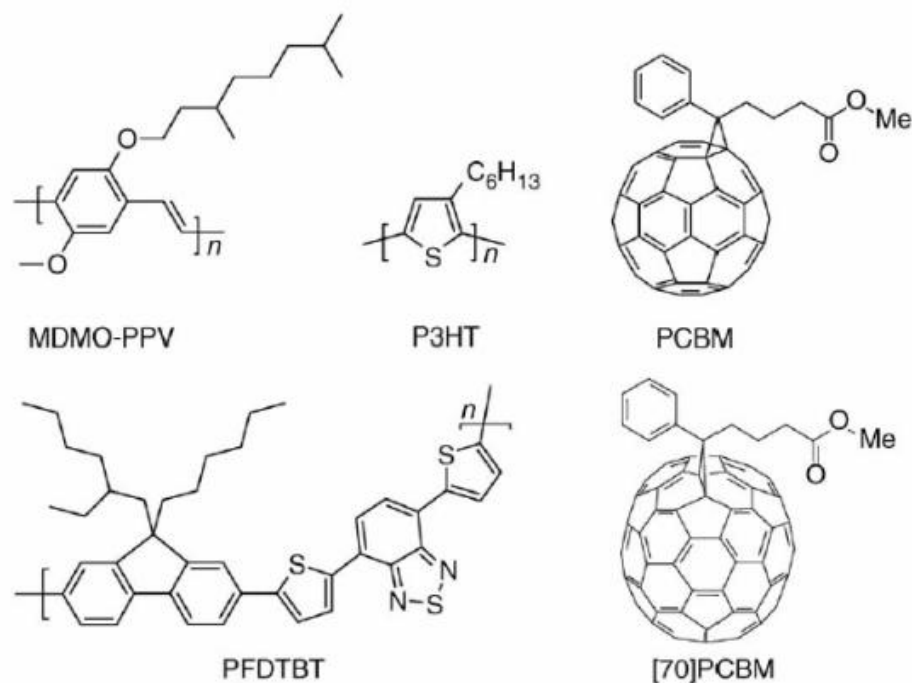


Figure 3.8. Examples of donor and acceptor materials used in polymer-fullerene bulk heterojunction (BHJ) solar cells [34].

Figure 3.8 shows some examples of organic semiconductors used in organic solar cells. A typical p-type organic molecule or polymer is a semiconductor which creates bonded electron-hole pairs or excitons. Excitons should transform into free charges with the help of an external electric field or via interfaces. Interfaces are regions where donor and acceptor phases contact to each other [34]. The buckminsterfullerene C_{60} is an electron acceptor. It is blended into electron-donating matrices with hole conducting properties for photoinduced electron-transfer reactions (Figure 3.9). Since the solubility of C_{60} is limited, its soluble derivative PCBM(phenyl-C61-butyric acid methyl ester) is widely used in polymer/fullerene solar cells [49]. If PCBM is mixed with a p-type semiconducting polymer such as P3HT, the heterojunctions are generated throughout the material. Photogenerated excitons need these heterojunctions to dissociate [34].

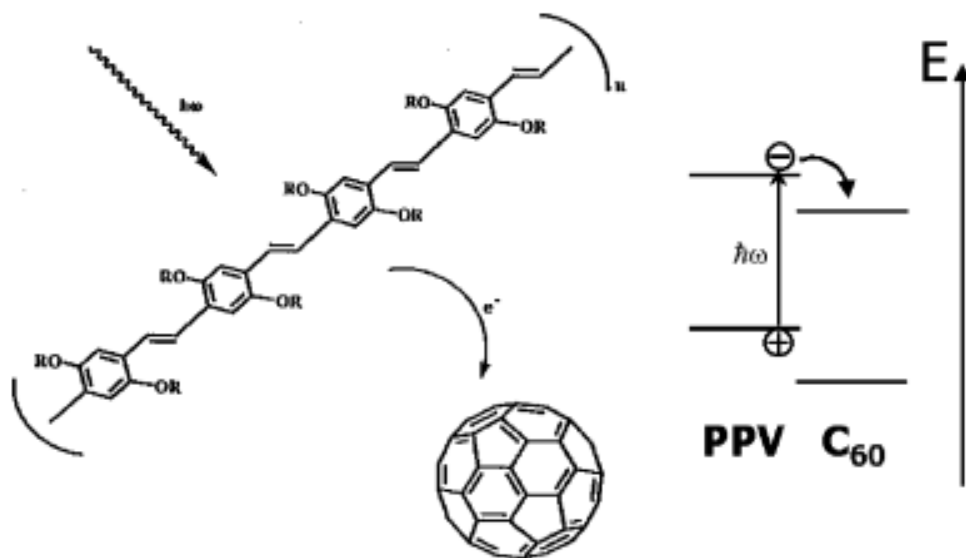


Figure 3.9. Illustration of the photoinduced charge transfer. Electrons are excited in the PPV (polyvinylpyrrolidone) polymer and transferred to the C₆₀ [49].

Photoinduced electron transfer from a donor to an acceptor-type organic semiconductor film introduces free charge carriers (positive charge carriers on the donor layer- p-type; and negative charge carriers on the acceptor layer-n-type). Donor-acceptor-type bilayer devices can work like p-n junctions [49].

PEDOT: PSS (Poly(3,4-ethylenedioxythiophene) poly(styrenesulfonate)) is used extensively in organic solar cells (Figure 3.10) [1, 48]. The PEDOT:PSS mixture is transparent in the visible region. The mixture is effectively used for the processes of transporting holes to the anode and blocking electrons since its work function is high providing the formation of an ohmic contact with donor polymers [50]. Additionally, it is a hole conducting material applied on top of the ITO electrode [1, 48].

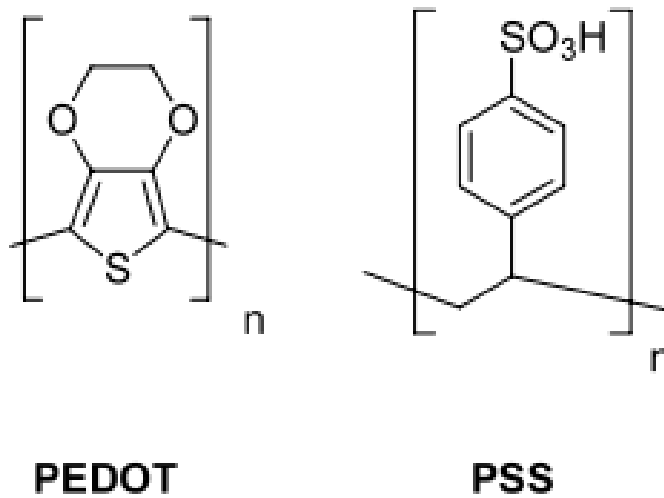


Figure 3.10. Chemical structures of PEDOT and PSS [1].

3.8. PREPARATION TECHNIQUES

Transparent anode, active layer, and cathode are layers of the organic photovoltaics. Several coating steps are needed for producing these layers [1].

Vacuum evaporation and solution processing techniques are the most commonly used thin film preparation techniques in the production of organic solar cells. Most polymer-based photovoltaic elements are solution processed at low temperatures because polymers decompose under excessive heat. There are some examples of printing/coating techniques used for production of polymer solar cells in the literature

- Spin-coating
- Doctor-blading
- Screen printing
- Inkjet printing [49].

A solution is casted on a layer which is placed onto a rotating substrate in spin coating method. When the rate of rotation increases, the thickness of the layer

decreases. Homogenous thicknesses below 100 nm can be obtained by this technique. Two preconditions for spin coating are spinable resistivity of layer-building material and solubility of the layer material in a solvent. It is a convenient method for deposition of organic polymers and biopolymers [20].

Printing techniques offer deposition of the material only in the areas needed in the final device structure. Also, this techniques provide an easy integration of organic devices into other applications.

Roll to roll coating method is another well-established coating method for high-speed processing of thin-film devices. Less damage to the films is an advantage, but lower process steps may be a disadvantage of this method. However it is not the scientists' first choice due to the need of large amounts of substrates and active material.

Screen printing is a very practical technique for research activities due to the requirement for less complex equipment and possibility to obtain more appropriate resolution level.

Pad printing is preferred to make a single print. This method provides printing on corrugated or curved surfaces. Lower viscosity requirement of ink as compared to screen printing, and possibility of using volatile solvents are the advantages of this method.

Doctor blading technique is mostly preferred for preparation of small prototypes on the laboratory scale. Relatively large areas can be coated by this technique. Only one-dimensional patterns are possible with doctor-blading [1].

Large-scale printing/coating techniques makes the production with low-energy consumption possible providing lower energy needed to produce a solar cell than the energy delivered by the same solar cell itself.

Vacuum evaporation is a choice for the deposition of thin films based on small molecules. In order to reduce contaminants like oxygen and water, a vacuum of $<10^{-5}$ mbar is applied.

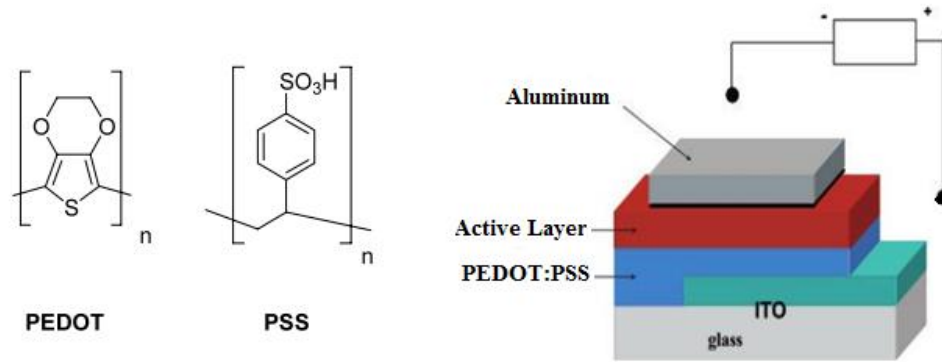


Figure 3.11. Schematic device structure for polymer/fullerene bulk heterojunction solar cells (top right). The active layer is sandwiched between two contacts: an indium-tin-oxide electrode coated with a hole transport layer PEDOT: PSS and a aluminum top electrode. Chemical structure of PEDOT: PSS (top left) [49].

The devices are fabricated in sandwich geometry (Figure 3.11). Transparent, conducting electrodes (glass or plastic covered with ITO) are used as substrates. On the transparent conducting substrate, PEDOT: PSS is coated. PEDOT: PSS layer improves the surface quality of the ITO electrode by reducing the probability of shorts and facilitating the hole injection/extraction. The active layers are coated using solution or vacuum deposition techniques. Top electrode is evaporated. In general, a lower work function metal as compared to ITO is used (such as aluminum) [49].

3.9. OPERATING PRINCIPLES

The process of conversion of light into electricity by an organic solar cell:

- Absorption of a photon
- Exciton creation
- Exciton diffusion
- Exciton dissociation
- Charge separation
- Charge transport within the organic semiconductor to the respective electrodes.

Organic materials have large band gaps, so they can absorb only a small portion of the incident solar light. On the other hand, organic materials have the absorption coefficients as high as 10^5 cm^{-1} , only 100 nm thickness is enough to absorb most of the photons [49].

Once the photoexcited electrons are transferred to an acceptor unit, then cation radical is resulted on the conjugated polymer backbone. The long lifetime of the charge transferred state and the high quantum efficiency of this process triggered the development of bulk heterojunction solar cells.

The primary photoexcitations in organic materials do not directly lead to free charge carriers but to coulombically bound electron-hole pairs, excitons. Strong electric fields are necessary for efficient dissociation of excitons. Such local fields can be supplied via externally applied electric fields as well as via interfaces. Strong electric fields are possible at an interface, because there are abrupt changes of potential energy. When the exciton reaches such an interface, photoinduced charge transfer can occur. Exciton diffusion length should be at the same order of magnitude as the donor acceptor phase separation length. If not, excitons recombine before reaching the interface and their energy is lost. Polymers and organic semiconductors have the exciton diffusion length around 5-20nm.

In order to separate photoexcited charge carriers into free charge carriers efficiently, conjugated polymers should be blended with electron acceptors, such as fullerene derivatives [49].

The created charges need to be transported to the corresponding electrodes during their lifetime. This can be done by one low-work function metal for the collection of electrons and one high-work function metal for the collection of holes. The concentration gradients of the respective charges can be another driving force.

Charge carriers are extracted from the device through two selective contacts. One of them is a transparent ITO, which has a work function that matches the HOMO levels of the conjugated polymers (hole contact), and the other one is an evaporated aluminum metal contact with a work function of around 4.3 eV that matches the LUMO levels of the acceptor PCBM (electron contact) [49].

3.10. ORGANIC PHOTOVOLTAIC DEVICE ARCHITECTURES

Photovoltaic devices consisting of thin films of organic semiconductors are defined as organic solar cells. In a bilayer device (Figure 3.12 (a)) an electron-donating layer and an electron-accepting layer of two different organic semiconductors generates a planar junction. Excitons generated by light dissociate into charge carriers at the planar junction, then they are collected at the corresponding electrodes [51].

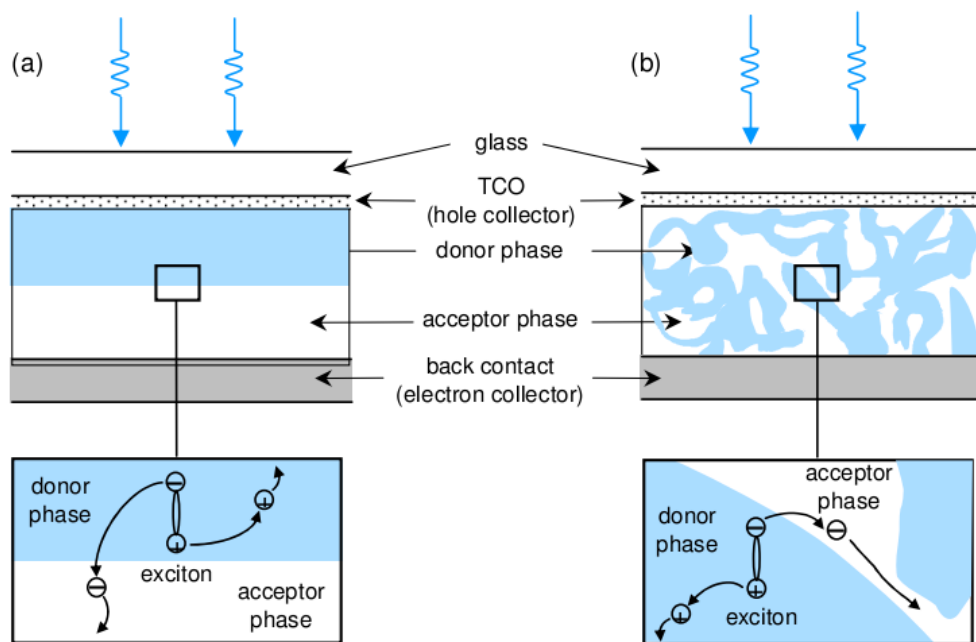


Figure 3.12. Architectures of organic photovoltaic cell. (a) Bilayer cell, (b) Bulk heterojunction cell [51].

3.10.1. Bilayer Devices

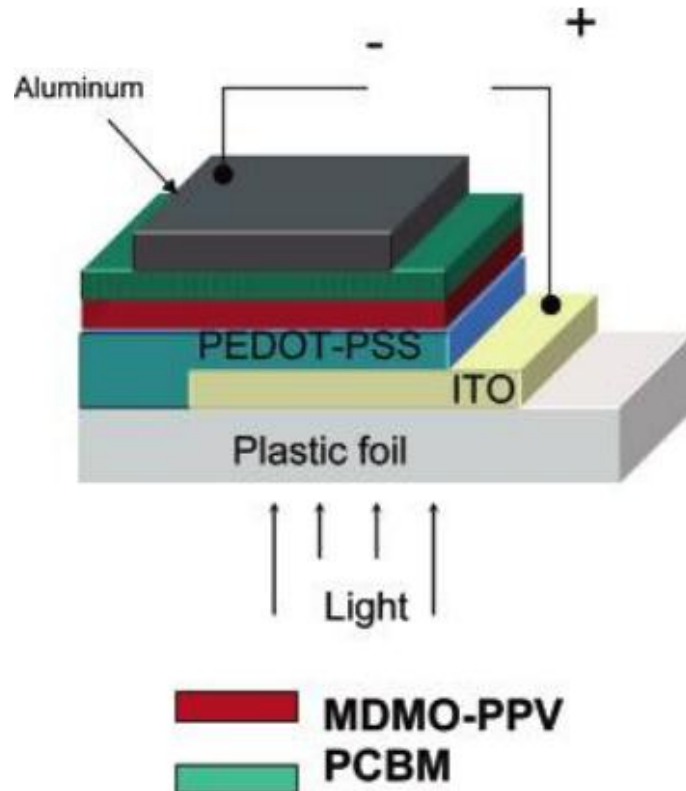


Figure 3.13. Bilayer configuration in organic solar cells [49].

Sequentially piled p-type and n-type semiconductors form a bilayer device. All excitons can not reach the heterojunction interface. Only the ones created within a distance of 5-20 nm from the interface cause the loss of absorbed photons further away from the interface and low quantum efficiencies. The charge generation in 5-20 nm around the donor-acceptor interface limits the efficiency [49].

3.10.2. Bulk Heterojunction (BHJ) Devices

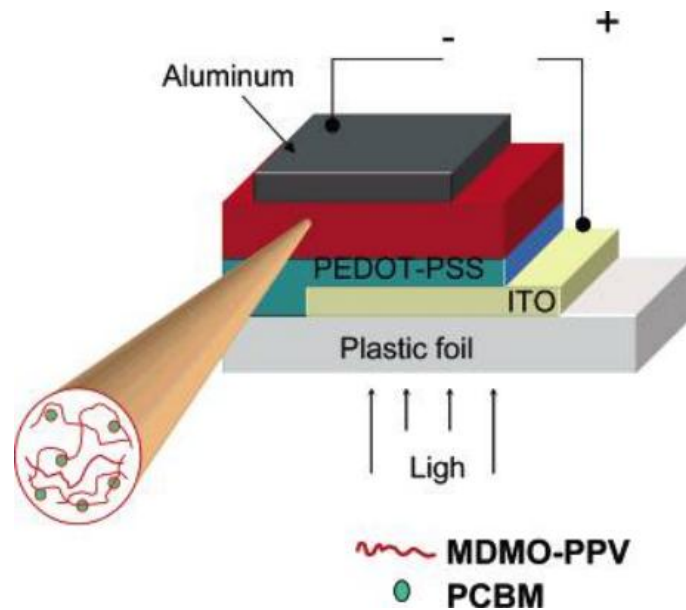


Figure 3.14. Bulk heterojunction configuration in organic solar cells [49].

A blend of the donor and acceptor phases which have phase separation of 5-20 nm, form a bulk heterojunction device creating a nanoscale interpenetrating network. The exciton diffusion length from the absorbing site is longer than each interface. Increased interfacial area between the donor and acceptor phases in the bulk heterojunction device results in improved efficiency in solar cells. The donor and acceptor phases are completely separated in bilayer devices, but they are intimately intermixed in bulk heterojunction devices creating a nanoscale interpenetrating network. This makes bulk heterojunction devices much more sensitive to the nanoscale morphology than bilayer devices [49].

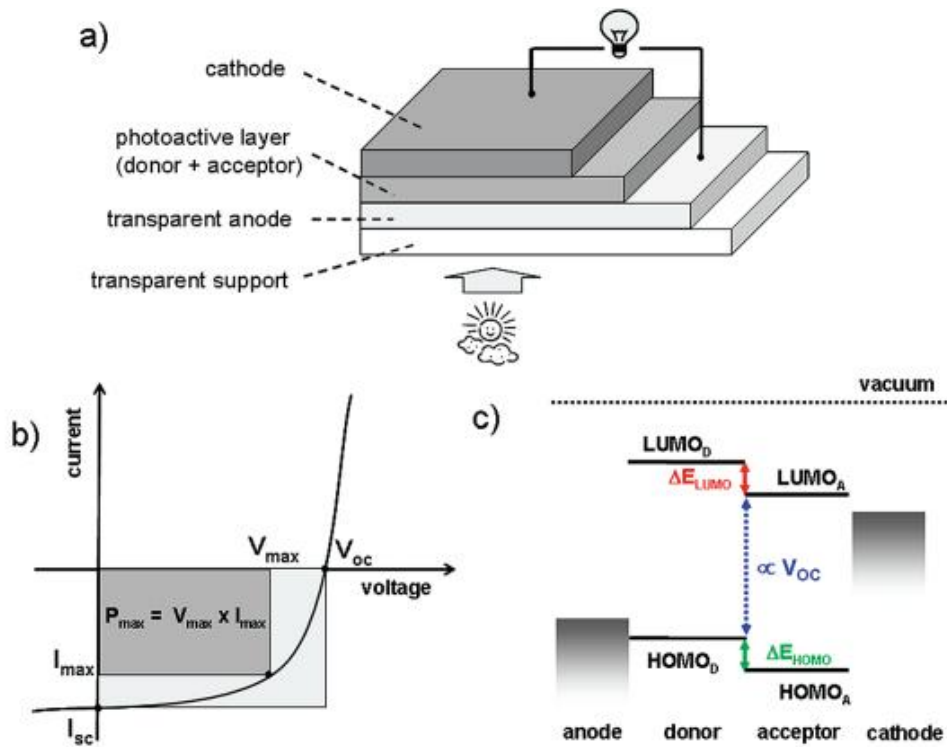


Figure 3.15. (a) Typical architecture of a single-junction polymer solar cell; (b) Current-voltage curve under illumination; (c) Energy levels diagram. The photovoltaic parameters extracted from the current-voltage curve; short-circuit current (I_{sc}); open-circuit voltage (V_{oc}); maximum output power (P_{max}) [52].

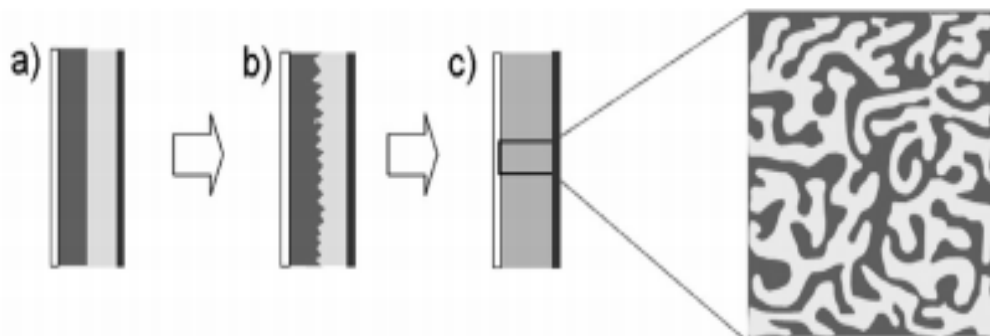


Figure 3.16. Structure of the photoactive layer (dark grey, donor; light grey, acceptor; white, anode; black, cathode). (a) bilayer heterojunction; (b) diffused bilayer heterojunction; (c) bulk heterojunction [52].

3.11. EXCITONS

3.11.1 Exciton Formation

Excitons are coulombically bound electron-hole pairs occurred in the active layer of solar cells after the absorption of light. The efficiency of absorption is related to the optical properties of organic materials. High absorption coefficients of organic materials are needed for high light absorption [48]. First, the donor polymer material absorbs incident photons with energies $h\nu$. Then, the electrons excite from the HOMO level to the LUMO level creating excitons [2]. The created excitons have binding energies in the range of 200-500 meV [2].

3.11.2. Exciton Diffusion

The created excitons should diffuse to the donor and acceptor interface to be separated into negative and positive charges. Since excitons are neutral, diffusion is not affected by any electric field but via random motions driven by the drift of concentration. Exciton diffusion lengths are around 5-20 nm for most conjugated polymers, then recombination takes place [2, 48]. If the exciton diffusion length is longer, the possibility of excitons to reach interfaces increases and photovoltaic effects rises [48]. Excitons that recombine do not make a contribution to the photocurrent [2, 48].

3.11.3. Exciton Dissociation

In order to dissociate excitons, extra driving forces are needed, as there is strong Coulombic interactions between electron and hole of an exciton and organic materials have low dielectric constant. Built-in electric field or heterojunction within a organic photovoltaic device generate these driving forces. While built-in electric field fails generally to dissociate the excitons into a hole and an electron, BHJ devices provide sufficient energy to dissociate them. The energy difference between the LUMO levels of the donor and the acceptor at the donor/acceptor

interface is the main driving force. However, the dissociation of excitons occurs at donor/acceptor interfaces and also material/organic interfaces [48].

3.12. CHARACTERIZATION OF A SOLAR CELL DEVICE

Short-circuit current (I_{sc}), open-circuit voltage (V_{oc}) and fill factor (FF) are three characteristic parameters used to characterize solar cells [34].

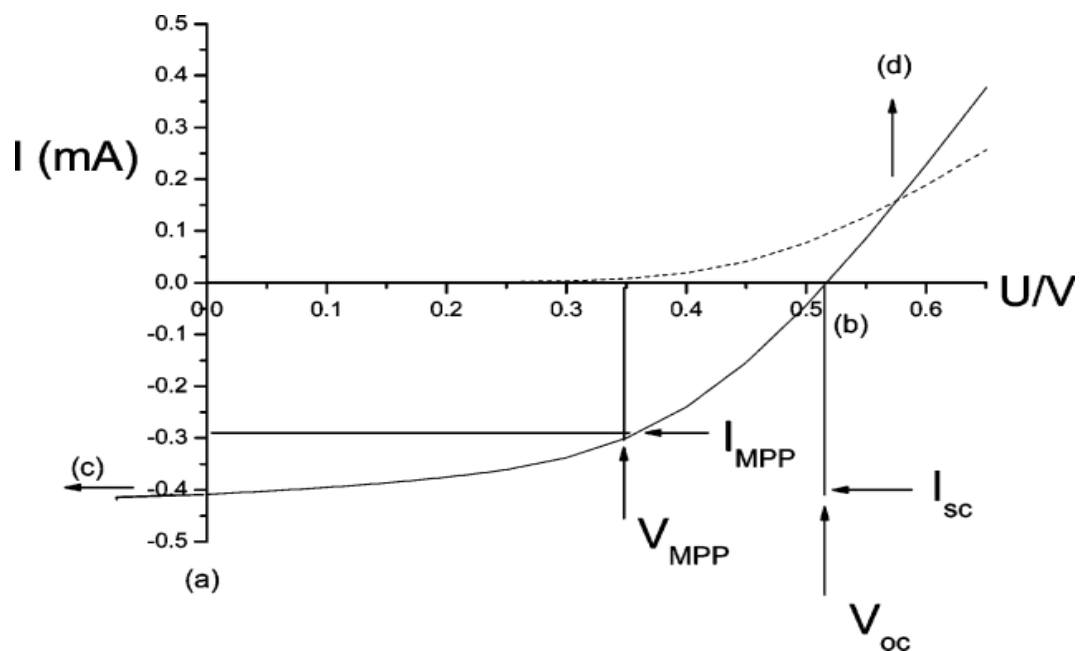


Figure 3.17. Current-voltage (I-V) curves of an organic solar cell. Almost no current flows in the dark [53].

The characteristic intersections with the abscissa and ordinate are the open circuit voltage (V_{oc}) and the short circuit current (I_{sc}), respectively. The largest power output is determined by the point where the product of voltage and current is maximized. Division of P_{max} by the product of I_{sc} and V_{oc} yields the fill factor FF [49, 53].

V_{oc} = open circuit voltage

I_{sc} = short circuit current

FF= fill factor

P_{in} = incident light power density (the light intensity is standardized at 1000 W/m² with a spectral intensity distribution matching that of the sun on the earth's surface at an incident angle of 48,2°, which is called AM 1,5 spectrum)

I_{mpp} and V_{mpp} = current and voltage at the maximum power point.

Efficiencies of organic photovoltaic devices are expressed by three methods.

- External quantum efficiency (η_{EQE}) or incident photon to current efficiency (IPCE): It is the ratio of the number of electrons collected by photovoltaic cells to the number of incident photons.

$$\eta_{EQE} = \frac{1240 \times J_{sc}}{\lambda \times P_{in}} \text{ (If the device is illuminated by a monochromatic light)}$$

- Internal quantum efficiency (η_{IQE}) or absorbed photon to current efficiency (APCE): It is the ratio of number of carriers collected at an electrode to the number of photons absorbed in the device.

$$\eta_{IQE} = \eta_{EQE} / (1 - T - R)$$

- Total conversion efficiency (η) or power conversion efficiency (PCE).

$$\eta = \frac{V_{oc} \times I_{sc} \times FF}{P_{in}} [48].$$

3.12.1. Open Circuit Voltage

It is the maximum available voltage determined by the difference of the quasi Fermi levels of the two charge carriers, that is, n-doped semiconductor energy level and p-doped semiconductor energy level in a p-n junction. In organic solar cells, the open circuit voltage is dependent on the HOMO level of the donor (p-type semiconductor quasi Fermi level) and the LUMO level of the acceptor (n-type semiconductor quasi Fermi level) [49]. It can also be determined as the voltage generated by the device with infinite resistance [53].

Open circuit voltage is affected by the morphology of the active layer in the polymer fullerene bulk heterojunction solar cells.

Interfacial effects at the metal/organic semiconductor interface change the work function of the electrodes and influence the open circuit voltage [49].

3.12.2. Short Circuit Current

It is determined by the product of photoinduced charge carrier density and the charge carrier mobility within the organic semiconductors. It can be calculated by using the Formula below:

$$\text{➤ } I_{sc} = ne\mu E$$

n = density of charge carriers (assuming the 100 % efficiency for the photoinduced charge generation in a bulk heterojunction mixture, n is the number of absorbed photons per unit volume)

- e = elementary charge
- μ = mobility
- E = electric field[49].

3.12.3. Fill Factor

It is determined by the charge carriers reaching the electrodes, when the built-in field is lowered toward the open circuit voltage [49]. It can be also defined as the ratio of the maximum power delivered by the solar cell to product $J_{sc} \cdot V_{oc}$. It can be derived from the current-voltage characteristics of a solar cell [35]. The series resistances influence the filling factor and should be minimized. Finite conductivity of the ITO substrate limits the fill factor on large area solar cells [49]. The fill factor does not depend on the area of the device [36].

$$FF = \frac{I_{mpp} \cdot V_{mpp}}{I_{sc} \cdot V_{oc}}$$

CHAPTER 4

PHOTOVOLTAIC DEVICE PREPARATION BY ADDING GOLD NANOPARTICLES

4.1. INTRODUCTION

The solar cells are devices converting sunlight into electricity [2]. In 1954, the first solar cells with single crystalline silicon as an active material were developed at Bell Laboratories [48]. Later, solar cells with active material in the form of polycrystalline or amorphous film were developed [48]. Significantly high power conversion efficiencies (ca % 25) can be obtained with silicon-based solar cells [2, 3, 48]. However, the need for elevated temperature, high vacuum, and numerous lithographic steps to produce these inorganic semiconductor-based photovoltaics result in high production costs and energy consumption [2]. Therefore, there is an active research on producing new efficient, low-cost photovoltaic devices. The polymer-based photovoltaic devices provide the possibility of simple and cost effective way of producing energy from sun [3].

Second generation solar cells (organic polymer-based solar cells) were first developed in 1959 to reduce costs and simplify the process [2, 48]. Their fabrication does not require high cost materials and complicated experimental steps. They can be produced simply by deposition of photoactive material as a thin film on substrates [2]. Therefore, they are more affordable compared to the first generation solar cells. Besides, second generation solar cells have the advantage of room temperature processing and mechanical flexibility [1, 4]. The power conversion efficiencies of polymer-based solar cells were low when they were first developed due to the insufficiency of exciton dissociation [2, 48]. The discovery of

inserting donor/acceptor interface in them provided better device performances as high as 1 % [1, 2, 48]. In particular, producing a bulk heterojunction (BHJ) device by mixing a fullerene, C₆₀, derivative with a polymer donor, device performances have been enhanced considerably [5, 54, 55]. The polymer-fullerene-based BHJ solar cells have the advantage of potential fabrication to large areas and facile manufacturing processes. However, there is a competition between the sweep-out of the photogenerated carriers and charge recombination within the BHJ film resulting from low mobility of BHJ materials [3]. Number of charges reaching to the electrode are needed to be increased [3]. This can be achieved by enhancing the absorption of light by BHJ film without increasing the film thickness.

Metallic nanoparticles (NPs) such as Au NPs are candidates for enhancing the power conversion efficiencies of organic solar cells by their localized surface plasmon resonance and their ability of trapping the light in the film [3, 7-9, 56]. The localized surface plasmon resonance provides an enhancement in local electromagnetic fields resulting an improvement in the optical properties of the nanostructure devices [57, 58]. Trapping the light in the film by scattering and reflecting provides an increase in the optical path length. Thus, they provide enhancement in the absorption of light and the photogeneration of mobile carriers, and thereby, may increase the power conversion efficiency [3]. Recently, integration of nanoparticles to polymer-based solar cells has become an active field of research. Nanoparticles with different morphologies (i.e. wire, rod, sphere) have been used to enhance electron transportation and increase light trapping [3, 37, 42-47].

In this work, we demonstrated the effect of the incorporation of gold nanoparticles (rods and stars) into the buffer (PEDOT:PSS) layer of organic solar cells. Using solution chemistry, we synthesized gold nanorods which have aspect ratio of ca. 4, and gold nanostars which have tip to tip distance of ca. 140 nm. These Au nanoparticles were blended into PEDOT:PSS layer with different volume ratios. The increase of short-circuit current and power conversion efficiency were obtained with an addition of optimum amount of Au nanoparticles into the buffer layer. At

the optimized blend ratio, we obtained 2.88 % power conversion efficiency (PCE) and 11.36 mA/cm² short-circuit current density (J_{sc}) for gold nanostars (3 vol %), and 1.67 % PCE and 6.76 mA/cm² J_{sc} for reference device prepared without adding any gold nanostars. Also, 2.54 % PCE and 11.56 mA/cm² J_{sc} were achieved for gold nanorods (10 vol %). These values are significantly higher for the ones observed for the reference device (1.11 % PCE and 3.74 mA/cm² J_{sc}) under the same conditions.

4.2. EXPERIMENTAL DETAILS

4.2.1. Preparation of Gold Nanoparticles

4.2.1.1. Materials

Gold (III) chloride trihydrate (HAuCl₄·3H₂O), sodium borohydrate (NaBH₄), ascorbic acid (AA), silver nitrate (AgNO₃), and sodium citrate (Na-citrate) were purchased from Sigma-Aldrich. Cetyltrimethylammonium bromide (CTAB) was purchased from Fluka. ITO coated glasses were purchased from VisionTek. Ultra-pure water (18 Ω) was used for all the experimental solutions.

4.2.1.2. Preparation of Gold Nanorods

i. Preparation of Seed Solution

In order to prepare the seed solution, 1.25 mL of an aqueous 0.002 M HAuCl₄·3H₂O and 2.74 mL ultra-pure DI water were added in a test tube. Then, 3.76 mL of a 0.2 M CTAB solution was added onto the mixture. After mixing, 0.9 mL of a 0.01 M ice-cold NaBH₄ solution was added and the color of the solution turned from orange to light-brown color. The solution was kept at room temperature in water bath for 2 hours [59].

ii. Preparation of Growth Solution

The concentrations of $\text{HAuCl}_4 \cdot 3\text{H}_2\text{O}$, CTAB, Ag^+ , L-ascorbic acid, and molar ratio of L-ascorbic acid to $[\text{AuCl}_4^-]$ were adjusted as 4×10^{-4} M, 9.5×10^{-2} M, 6×10^{-5} M, 6.4×10^{-4} M, and 1.6:1, respectively and added in a test tube in that order. Then, the seed solution was added into the mixture. Final ratio of $[\text{Au}]_{\text{seed}}$ to gold concentration $[\text{AuCl}_4^-]$ was 1/320. Finally, the solution was mixed for 20 s and left undisturbed at room temperature for 24 hours [59].

4.2.1.3. Preparation of Gold Nanostars

Gold colloids, purchased from Ted Pella, was used as seed solution. In order to synthesize Au nanostars 0.2 mL of an aqueous 0.01 M solution of $\text{HAuCl}_4 \cdot 3\text{H}_2\text{O}$ was added to 4.75 mL of a 0.1 M CTAB solution in a test tube. The solution was gently mixed. Then, 0.03 mL of a 0.01 M AgNO_3 solution and 0.032 mL of a 0.1M AA solution were added in that order, resulting a colorless solution. Finally, 10 μL of commercially available seed solution was added. After the reaction mixture was gently mixed, the solution was kept at room temperature and undisturbed for 3 hours. The color of the nanorod solution became blue-purple indicating the formation of gold nanostar [12].

4.2.2. Photovoltaic Device Preparation

Photovoltaic devices based on conjugated polymers with a blend of Au nanoparticles were prepared as shown in Figure 4.1 (a). ITO (indium-tin-oxide) coated glass, which is a transparent, conductive electrode, was used as a substrate. First, ITO coated glass was cleaned with isopropanol, acetone and pure water to remove the impurities and dust. Thus, the undesirable change in the work function of ITO was prevented. The glass was then treated with an oxygen plasma for 10 minutes to revise the ITO surface. Then, PEDOT: PSS mixed with different types of Au nanoparticle solutions having different concentrations were blended over the ITO. This PEDOT: PSS with Au nanoparticles was spincoated onto the ITO in a thickness of 40 nm. Then the ITO glass with the PEDOT: PSS with Au nanoparticle

was taken in a glove box and heated on a digitally controlled hot plate at 90 °C for 4 minutes. A mixture of P3HT: PCBM dissolved in 1 mL of chlorobenzene was prepared and spincoated onto the PEDOT: PSS. Then, coated ITO glass was placed in a vacuum chamber in the glove box system for evaporation of Al cathode. Al is evaporated at very high temperature such as 660 °C, at which polymers used for producing device can easily be degraded. Thus, the vacuum chamber in the glove box was used to provide low pressure such as 10^{-5} mmHg, thereby Al could be evaporated at lower temperatures. At the end of evaporation step, the organic solar cells were annealed in the glove box at 90 °C for 4 minutes. In the experiments, the organic solar cells were prepared by using gold nanoparticles and without adding gold nanoparticles to compare the devices under the same conditions.

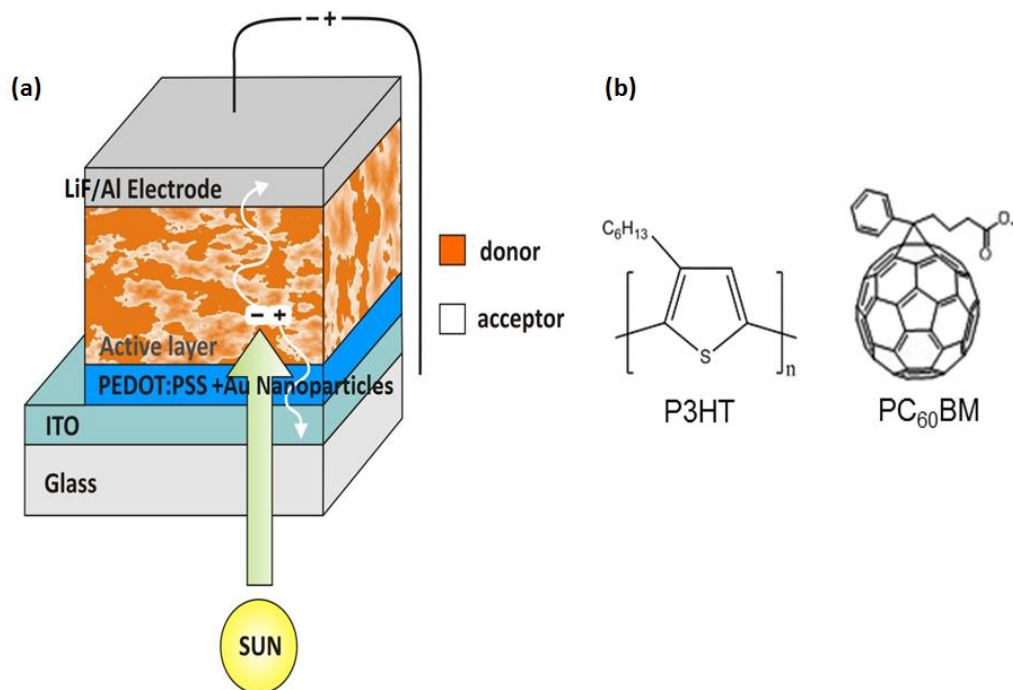


Figure 4.1. (a) Schematic draw of a photovoltaic device, (b) Molecular structures of photovoltaic materials (P3HT: donor; PC₆₀BM: acceptor)

4.3. CHARACTERIZATION

UV-vis absorption spectra, scanning electron microscopy (QUANTA 400F Field Emission SEM), and transmission electron microscopy (JEOL JEM 100 CX II TEM) were used to characterize the gold nanoparticles. Current-density and voltage were measured in dark and under illumination (AM 1.5G, 100 mW/cm²) with a Keithley 2400 sourcemeter calibrated for AM 1.5 illumination with a light intensity of 100 mW/cm².

4.4. RESULTS AND DISCUSSION

In this study, gold nanoparticles were added to the buffer layer in polymer based solar cell. Device efficiencies were evaluated for the addition of gold nanoparticles with two different morphologies; rod and star. Nanoparticles were synthesized by seed mediated growth method in aqueous media as described in literature [12, 59]. Figure 4.2 shows TEM images of Au nanorods. The images show uniformly sized gold nanorods with aspect ratio of ca. 4. SEM images of nanostars are demonstrated in Figure 4.3. The particles have three-dimensional structures with various number of tips growing out of the particle core. The gold nanostars have tip to tip distance of ca. 140 nm. The optical properties of these particles were characterized by UV-Vis spectroscopy. The absorption spectra of gold nanorods show two strong plasmon bands with maximum intensities at around 540 nm and 800 nm (Figure 4.4). On the other hand gold nanostars demonstrate very broad plasmon bands around 600 nm and 900 nm. The broadness is most likely due to the non-uniform nature of these particles (Figure 4.5).

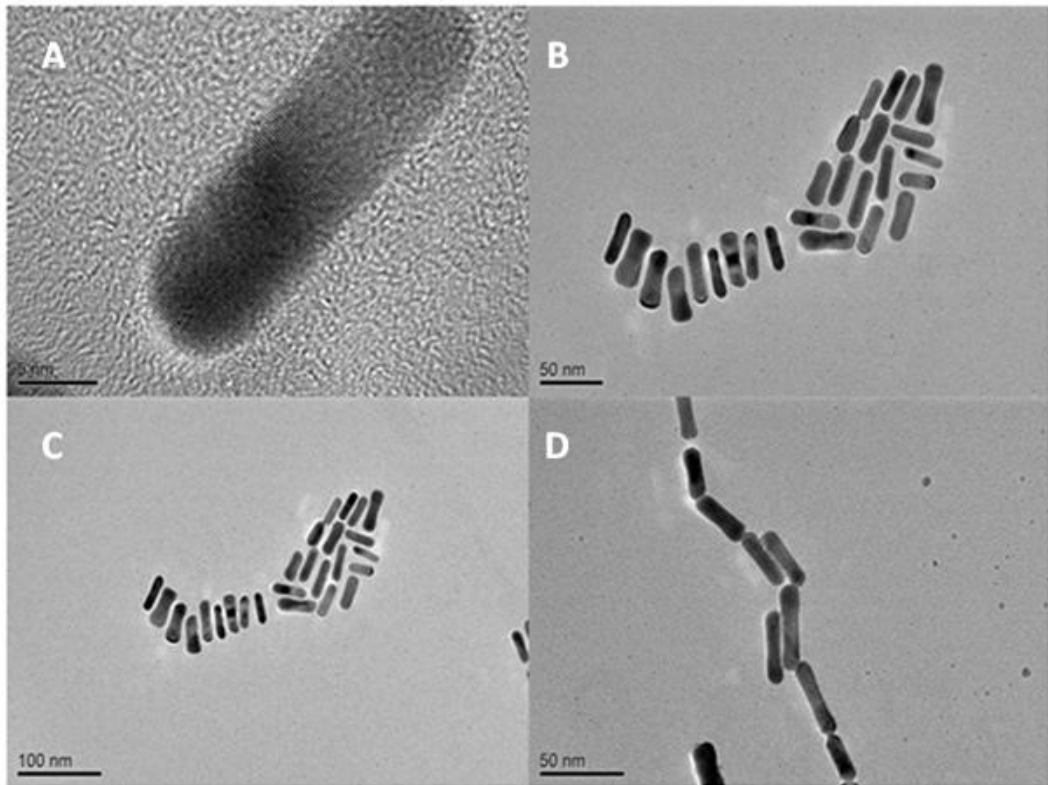


Figure 4.2. TEM images (A-D) of synthesized gold nanorods.

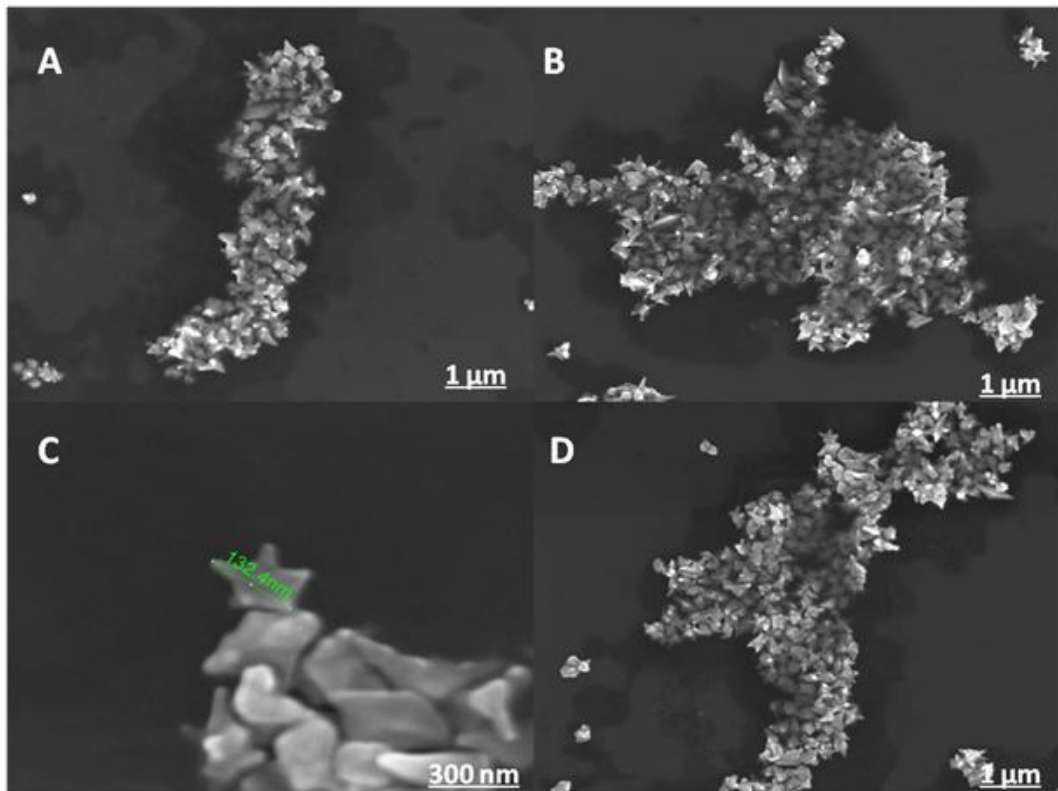


Figure 4.3. SEM images of synthesized gold nanostars.

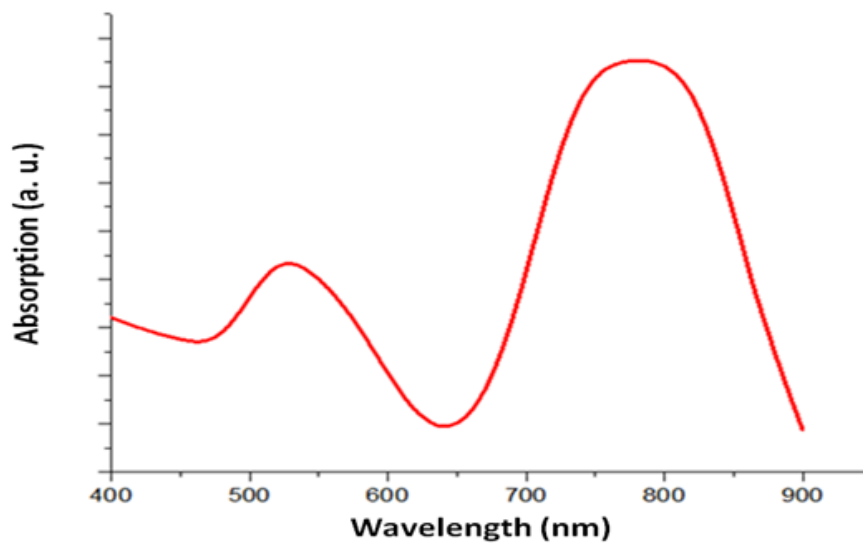


Figure 4.4. UV-Vis absorption spectrum of the synthesized gold nanorods in water.

Organic materials have large band gaps resulting the absorption of a very small portion of the solar light. Gold nanorods and nanostars can absorb the light in the near IR region where no absorption by organic polymers occurs. Therefore, the observed increase in the photocurrent is most likely due to the localized surface plasmon resonance of gold nanoparticles and reflected light from the gold nanoparticles back to the active layer.

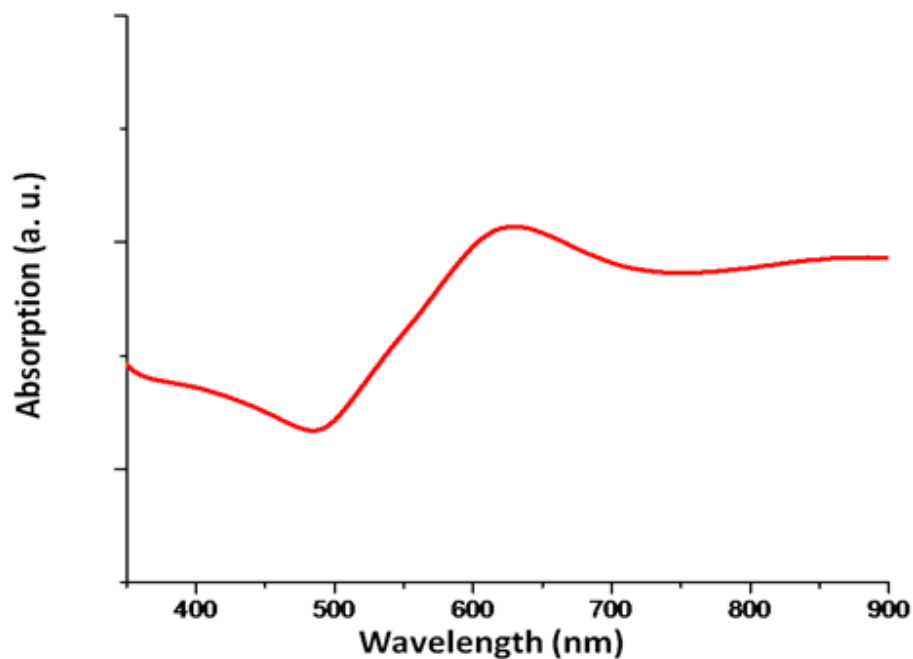


Figure 4.5. UV-Vis absorption spectrum of the synthesized gold nanostars in water.

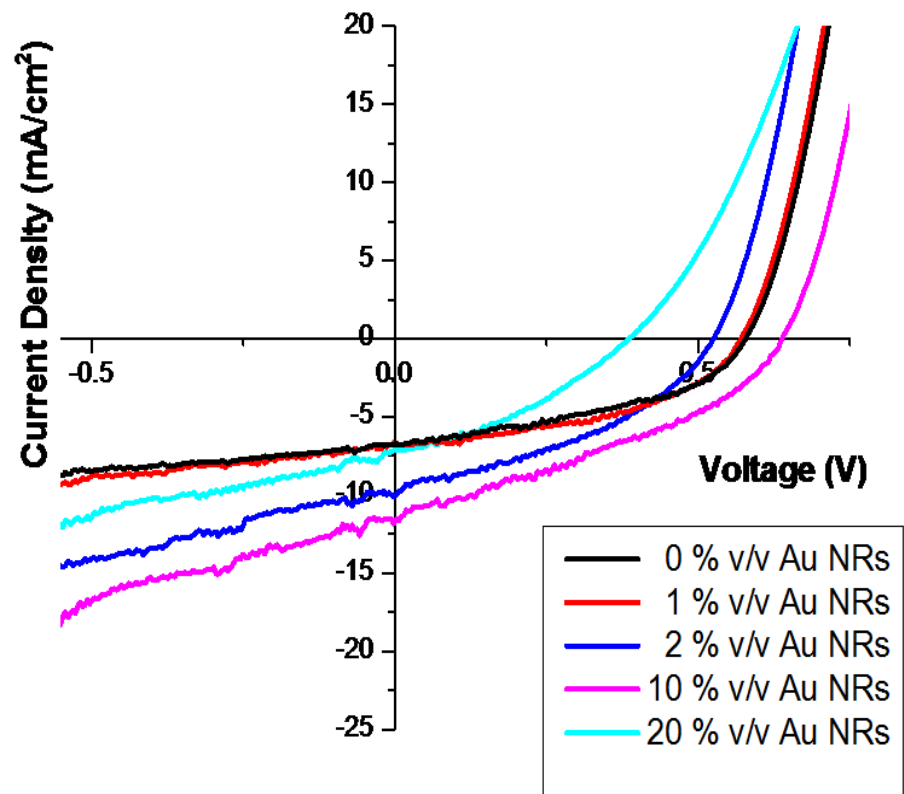


Figure 4.6. Organic solar cell characteristics based on the volume percentage of nanorods in the PEDOT:PSS layer measured under illumination. The best efficiency and the highest current value were observed when 10 vol % of gold nanorod added to the solution.

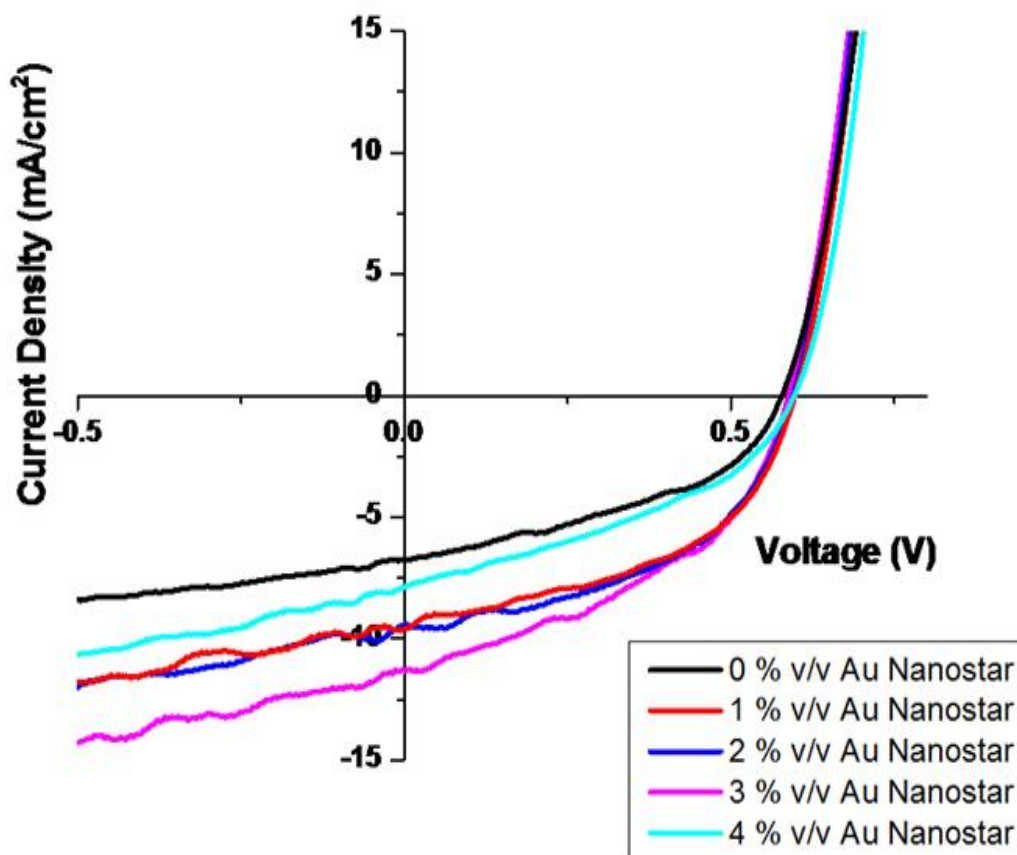


Figure 4.7. Organic solar cell characteristics based on the volume percentage of nanostars in the PEDOT:PSS layer measured under illumination. The best efficiency and the highest current value were observed when added 3 vol % of gold nanostar solution.

J-V (Current density-voltage) characteristics were measured for samples prepared from different concentrations of gold nanorod and gold nanostar solutions to determine the influence of concentration on the efficiency (Figure 4.8, and 4.9). The increase in current value was observed upon addition of gold nanoparticles.

Organic solar cells produced by adding gold nanoparticles show improved device performances compared to the reference device produced by without adding any gold nanoparticles. The work function of Au nanoparticles added into buffer layer of BHJ solar cells is close to the HOMO (highest occupied molecular orbital) energy level of P3HT providing a small energy barrier thus facilitating the extraction of holes. Besides, addition of large gold nanoparticles may lead to lowering of series

resistance. This could lead to passing the holes through less interfaces in systems with large gold nanoparticles. Moreover, decreased hole injection barrier, the energy difference between E_{HOMO} and zero binding energy may be observed in the BHJ solar cells produced by adding gold nanoparticles. This makes hole transfer from the HOMO energy of P3HT to the ITO electrode easier and reduces the possibility of electron-hole recombination. This might be a reason for the increase of J_{sc} .

Table 4.1. Photovoltaic parameters of organic solar cells incorporated in different concentrations of gold nanorods and gold nanostars (FF: Fill factor, J_{sc} : current density, V_{oc} : open circuit voltage, and PCE: power conversion efficiency).

Concentration of Au Nanorods (by volume)	FF	J_{sc} (mA/cm ²)	V_{oc} (Volt)	PCE (%)
0 %	0.43	6.76	0.58	1.67
1 %	0.45	6.84	0.57	1.77
2 %	0.38	9.89	0.52	1.98
10 %	0.35	11.56	0.63	2.54
20 %	0.36	7.27	0.38	0.99
Concentration of Au Nanostars (by volume)	FF	J_{sc} (mA/cm ²)	V_{oc} (Volt)	PCE (%)
0%	0.43	6.76	0.58	1.67
1 %	0.48	9.66	0.59	2.72
2 %	0.47	9.92	0.59	2.75
3 %	0.43	11.36	0.59	2.88
4 %	0.39	7.87	0.59	1.80

The device characteristics are summarized in Table 4.1. It is obvious that addition of gold nanoparticles into PEDOT:PSS layer of a BHJ solar cell increases the PCE as compared to the polymer based organic solar cells produced without adding any gold nanoparticles. We optimized the blend ratio 3 vol % for gold nanostars, 10 vol % for gold nanorods. 1.11 % and 1.67 % PCE was observed for the reference cell

(without adding any gold nanoparticles). The values increased significantly to 2.54 % and 2.88 % upon addition of gold nanorods and nanostars, respectively. The values of J_{sc} increased to 11.36 of mA/cm^2 J_{sc} for gold nanostars, and and 11.56 of mA/cm^2 for nanorods. Reference devices showed the values of J_{sc} ; 6.76 mA/cm^2 , and 3.74 mA/cm^2 prepared under the same conditions with devices producing by gold nanostars and gold nanorods, respectively.

The increase of PCE of organic solar cells produced by adding gold nanoparticles into PEDOT: PSS layer was previously reported [46, 60]. D. H. Wang et al. enhanced the PCE from 3.1 % to 3.51 %. L. Qiao et al. found the PCE from 1.99 % to 2.36 %. In our study, we increased the PCE from 1.67 % to 2.88 %. On the basis of these results, it can be said that the addition of gold nanoparticles into PEDOT:PSS layer of an organic solar cell improves the PCE significantly.

Local electromagnetic fields generated by gold nanoparticles and increase in the optical path length resulted from the trapping of sunlight in the film by gold nanoparticles provides an increase in short-circuit current and power conversion efficiency as well. When the distance between Au nanoparticles decreases, surface plasmon resonance strength increases. Additionally, roughness of the PEDOT:PSS layer might be increasing upon the increase of the concentration of Au nanoparticles. The interfacial area between the anode and the active layer is increasing through the increasing roughness facilitating hole collection at the anode. This may be another reason for an increase in short circuit current and an enhancement in fill factor.

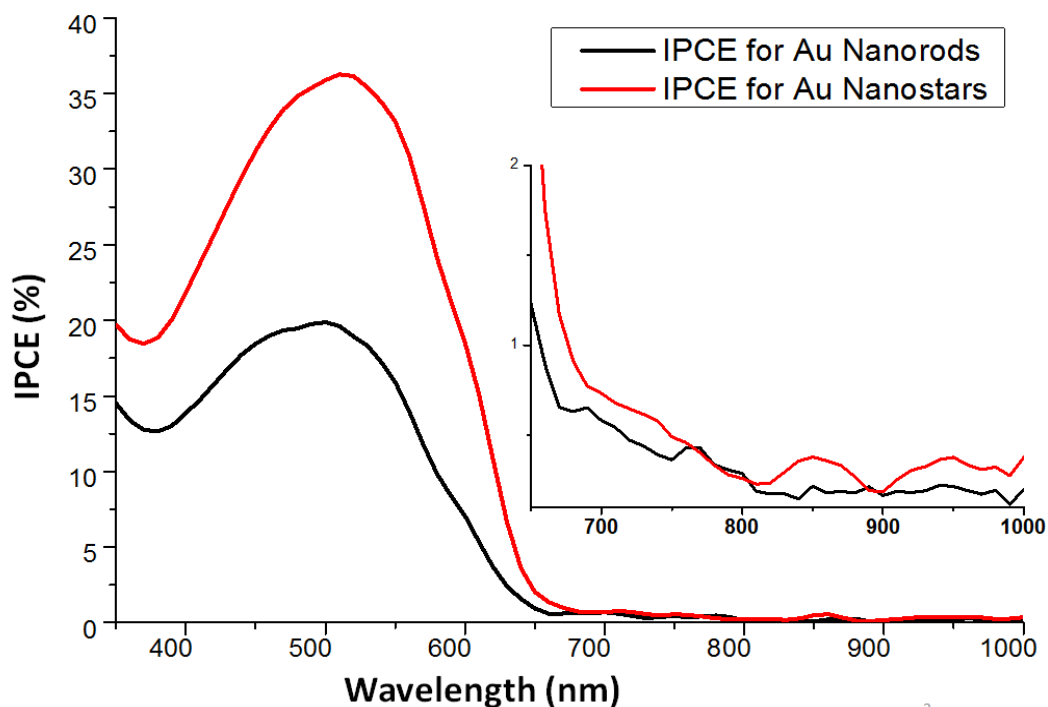


Figure 4.8. IPCE vs. wavelength (spectral response) of devices produced by adding gold nanorods and gold nanostars into PEDOT:PSS layer. Inset shows closer look at the region between 650 nm and 1000 nm indicating higher IPCE obtained with gold nanostars compared to nanorods.

The percentage of incident photons resulting in free charges collected through the electrodes of photovoltaic device is measured by incident photon-to-current efficiency (IPCE). Efficient light trapping, surface plasmon effect, and improved charge transport due to gold nanostars provides more enhancement in the IPCE spectra as compared to the devices produced by adding gold nanorods as shown in Figure 4.8. Our measured IPCE shows a wideband improvement from ~400 to 650 nm. A maximum IPCE of 20 % at 500 nm for devices produced by adding gold nanorods and 36 % at 510 nm for devices produced by adding gold nanostars were obtained. Comparison of IPCE data for devices prepared with gold nanorods and nanostars demonstrate that use of nanostars improve device performance significantly. Light absorption, resistance of electrodes, exciton dissociation rates and charge collection efficiencies affect the magnitude of IPCE. Combination of

factors like large size and branched structure of nanostars as well as their strong absorption in near IR region are most likely reasons making them better contributors for organic solar cells to enhance PCE compared to gold nanorods.

It was also noted that PCE and J_{sc} values increased systematically as the amount of gold nanoparticles were increased up to certain level (Table 4.1). These levels show optimum nanoparticle quantity to obtain maximum performance from the device for each nanoparticle type. PCE reach maximum value when 3 vol % of gold nanostar and 10 vol % of gold nanorod solution were used. The efficiency values decrease upon further addition of nanoparticle solution. At higher concentrations short circuit was observed. This is most likely due to increased electrical field produced by gold nanoparticles and increased contact of the particles. When concentration of gold nanoparticles increases, significant amount of sunlight is being absorbed by Au nanoparticles. The conduction between ITO and active layer decreases. This may be another reason of the reduced values of J_{sc} and PCE at higher concentrations.

We also measured the series resistance and the shunt resistance of devices produced by adding gold nanorods and gold nanostars and the ones without adding any gold nanoparticles to compare. We observed a decrease in series resistance and an increase in shunt resistance. J-V measurements indicated the reduction of series resistance from $4.3315 \Omega \text{ cm}^2$ (no NPs) to $4.0108 \Omega \text{ cm}^2$ for devices produced by adding gold nanorods. The value reduced to $3.7320 \Omega \text{ cm}^2$ for devices produced by adding gold nanostars. Reduced series resistance might be resulted from the ability of gold nanoparticles to reflect and scatter the incident light and increase the optical path length, thus improve the photocurrent generation and charge transport. Hole collection at the interface between PEDOT: PSS and P3HT: PCBM provides an enhancement in the PCE and a reduction in series resistance. J-V measurements also indicated the increase of shunt resistance from $0.1584 \Omega \text{ cm}^2$ (no NPs) to $0.2309 \Omega \text{ cm}^2$ for devices produced by adding gold nanorods. The value increased to $0.2496 \Omega \text{ cm}^2$ for devices produced by adding gold nanostars. The

increase in the shunt resistance is most likely due to the enhanced absorption of light and photocurrent generation through nanoparticles.

4.5. CONCLUSION

In conclusion, a series of BHJ solar cell produced by adding gold nanorods, and gold nanostars into PEDOT:PSS layer were prepared and an improvement in PCE were demonstrated.

Maximum PCE performance was observed when 10 vol % gold nanorods and, 3 vol % gold nanostars were added. Compared to the devices produced by adding gold nanostars, gold nanorods, and the ones produced without adding gold nanoparticles, the values of % 2.88 of PCE, and 11.36 of mA/cm² J_{sc} by adding gold nanostars, and % 1.67 of PCE, and 6.76 of mA/cm² J_{sc} without adding any gold nanoparticles; % 2.54 of PCE, and 11.56 of mA/cm² J_{sc} by adding gold nanorods, and % 1.11 of PCE, and 3.74 of mA/cm² J_{sc} without adding any gold nanoparticles were obtained under the same conditions.

The improvement of PCE results from surface plasmon resonance of gold nanoparticles and their ability to trap the light in the film for more time. Increase in the roughness of the buffer layer might be facilitating hole collection at the anode. This provides an enhancement in the short circuit current. However, PCE and J_{sc} values increased up to a certain level of the amount of nanoparticles. Then, they decreased and short circuit was observed at further increase of the concentration of Au nanoparticles. Absorption of significant amount of sunlight by gold nanoparticles might be the reason of decrease of PCE and J_{sc} values.

Future efforts will be concentrated on fabrication of BHJ solar cells by adding different types of gold nanoparticles such as gold nanospheres, and different kinds of nanoparticles such as silver nanoparticles.

CHAPTER 5

GROWTH OF BRANCHED GOLD NANOPARTICLES ON SURFACES

5.1. INTRODUCTION

Gold nanoparticles with anisotropic morphologies have attracted great deal of attention due to their unique optical and plasmonic properties. In particular, the ones with branched structures have strong absorptions in the near IR-regime and generate strong electric field strength at their tips [10-13]. The special optical properties of these nanoparticles make them useful in photonics, electronics as well as sensing, imaging and biomedical applications [10-12, 61].

Numerous solution based techniques were improved to synthesize anisotropic shaped gold nanoparticles [11, 12]. Most of them involves chemical reduction of a gold salt in the presence of surfactant molecule such as cetyltrimethylammonium bromide (CTAB) and poly-vinylpyrrolidone (PVP) [7]. Seed-mediated growth method is one of the most commonly used route that provide an access to prepare gold nanoparticles with different morphologies in aqueous media [62, 63]. This method is preferred because of its simplicity, control over nanoparticle morphology and high yield by manipulating parameters such as concentration of reactants and pH.

Nanoparticles should be stabilized on surfaces for utilizing them in desired applications. This can be achieved either by transferring nanoparticles synthesized in solutions onto substrates or growing them directly on surfaces. Seed mediated approach has been used to synthesize gold spheres, rods, and wires on different surfaces (i.e. mica, glass, ITO, Si) [64]. However, synthesis of branched gold

nanoparticles, which have superior optical properties, on surfaces have not been reported, yet.

In this part of the study, gold nanoparticles with branched morphologies were synthesized directly on glass, Si wafer, and ITO surfaces by using seed mediated growth method. The substrates studied are promising for further use in device applications [14]. Also, having branched nanoparticles with special optical properties grown on them make this system attractive for applications such as solar cells.

5.2. EXPERIMENTAL SECTION

5.2.1. Materials

Hydrogentetrachloroaurate (III) trihydrate ($\text{HAuCl}_4 \cdot 3\text{H}_2\text{O}$), ascorbic acid (AA), sodium borohydrate (NaBH_4), silver nitrate (AgNO_3), and sodium citrate dihydrate were all purchased from Sigma Aldrich. Cetyltrimethylammonium bromide (CTAB) was from Fluka. ITO coated glasses were purchased from VisionTek. Ultra-pure water was used for all the experimental solutions.

5.2.2. Preparation of Gold Seeds

Spherical gold nanoparticles were used as seeds. They were prepared by using a solution-based method described in the literature by Gole et al. [65]. First, 0.25 mL of 0.01M HAuCl_4 , 0.25 mL of 0.01 M Na-citrate, and 9.5 mL ultra pure water were added in a test tube and mixed. Then, 0.3 mL of 0.1 M ice-cold NaBH_4 was added into the mixture and mixed by rapid inversion for 2 minutes. The mixture was kept at room temperature. After 3 hours the citrate-stabilized 3.5 nm seed solution was ready for further use. Subsequently, 1.125 mL of 0.01 M HAuCl_4 , 0.25 mL of 0.1 M AA, and 5 mL of seed solution were added into 45 mL of 0.08 M CTAB in a test tube and mixed gently. Finally, 15 nm in diameter spherical gold nanoparticles were obtained [66].

5.2.3. Preparation of Branched Gold Nanostars

Schematic representation of synthesis of branched gold nanoparticles on substrates (i.e. indium-tin-oxide (ITO), glass, Si wafer) was illustrated in Figure 5.1. After cleaning processes of substrates by using water, acetone, and isopropanol, they were treated with a 0.01 % toluene solution of aminopropyltrimethyloxysilane (APTMS) for 30 minutes. Then, the substrates were washed with ethanol, ultra pure water and dried. The APTMS covered substrates were then immersed in the seed solution for different time periods (5 seconds-1 hour) and washed again with ultra pure water and dried. For the growth of nanostars, the substrates were immersed in a growth solution containing 4.75 mL of 0.1 M CTAB, 0.2 mL of 0.01 M HAuCl₄, 0.03 mL of 0.01 M AgNO₃, 0.032 mL of 0.1 M AA and kept in the solution undisturbed overnight. Finally, they were washed with ultra pure water and dried.

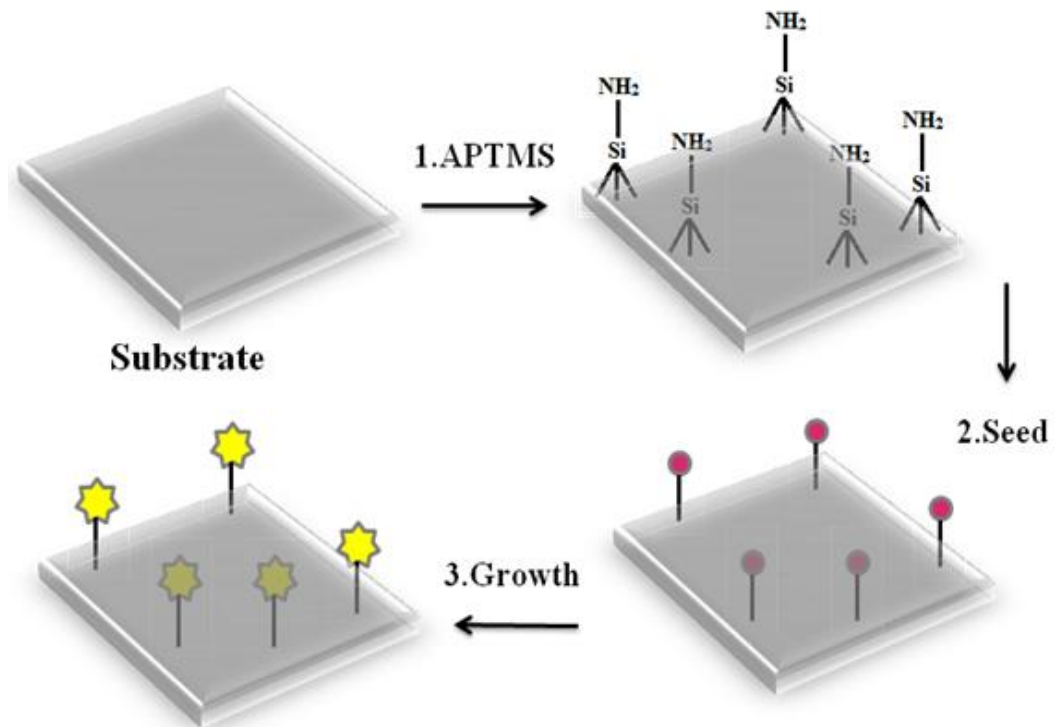


Figure 5.1: Schematic diagram of the growth process of branched gold nanoparticles on surface.

5.3. RESULTS AND DISCUSSION

In this work, branched gold nanoparticles were grown directly on three different substrates; glass, Si wafer and ITO. Figure 5.1 illustrates the growth process of the nanoparticles. The surface of the substrates were first coated with (3-Aminopropyl)trimethyloxysilane (APTMS) which function as a linker between substrate surface and gold nanoparticle. The molecule has a silane group which preferentially bind to the substrate surface and amine group which has tendency to attach gold nanoparticle surface with complex forming between nitrogen and gold nanoparticles [14]. The growth of branched nanoparticle on APTMS coated substrate was achieved with “seed mediated growth” based method [64]. Firstly, APTMS functionalized substrate surface was coated with a spherical gold nanoparticles, which serve as seeds for branched nanoparticles (Figure 5.2). Then, desired nanoparticles were grown by immersing the seed coated substrate to the growth solution. The change in color of substrate surface from colorless to purple indicates the formation of nanoparticles on the surface. Also, observation of no color change in growth solution suggests that no or very little nanoparticle formation in growth solution.

SEM analysis revealed that branched gold nanoparticles were successfully grown on glass, Si wafer, and ITO surfaces (Figure 5.3, 5.4, and 5.5). The analysis also showed the nanoparticles were not washed out after purification step followed by incubation of substrates in growth solution. This indicates existence of strong interaction between the substrate and the particles. The branched nanoparticles are presumably attached to APTMS coated substrate surface through Au-amine bonds, but there is no direct evidence for the surface interactions.

The nanoparticles have non-uniform morphologies with broad size distributions (between 300-700 nm) were formed on three of the substrates. Observation of no significant difference in both morphology and size distribution for nanoparticles grown on three different substrates indicates that substrate does not have

influence on the nanoparticle properties. On the other hand, difference in density (nanoparticle number per unit area) of nanoparticles on substrate surface was observed. This difference is notable when SEM images acquired at low magnification were compared (Figure 5.3 (C), 5.4 (C), 5.5 (C)). Branched nanoparticles were less densely grown on ITO compared to the ones on Si wafer and glass. Two reasons can be suggested for this observation: (i) gold nanoparticles are less tightly bound on the APTMS coated ITO surface and purification step removes significant amount of them from the surface, or (ii) APTMS is attached to ITO surface less effectively compared to the surface of glass and Si wafer. Thus, less Au seeds could be transferred to the surface and less number of branched nanoparticle formation took place. First reason is ruled out because gold nanoparticles are expected to make strong affinity with amine group of APTMS and density of nanoparticles on the surface will depend on the number of APTMS already exist to bind them to the surface. Therefore, possible weak interaction between APTMS and ITO is most likely reason for observing less branched nanoparticle formation on ITO.

Control of nanoparticle density grown on the substrate surface was also studied. Theoretically, altering the incubation time of substrate in seed solution will lead to control of seed deposition, thus number of nanoparticles formed on the surface. Incubation times from 5 seconds to 60 minutes was studied and results were evaluated with SEM analysis. However, the results showed no significant change in concentration of nanoparticles on the surfaces, suggesting very fast deposition of seed particles.

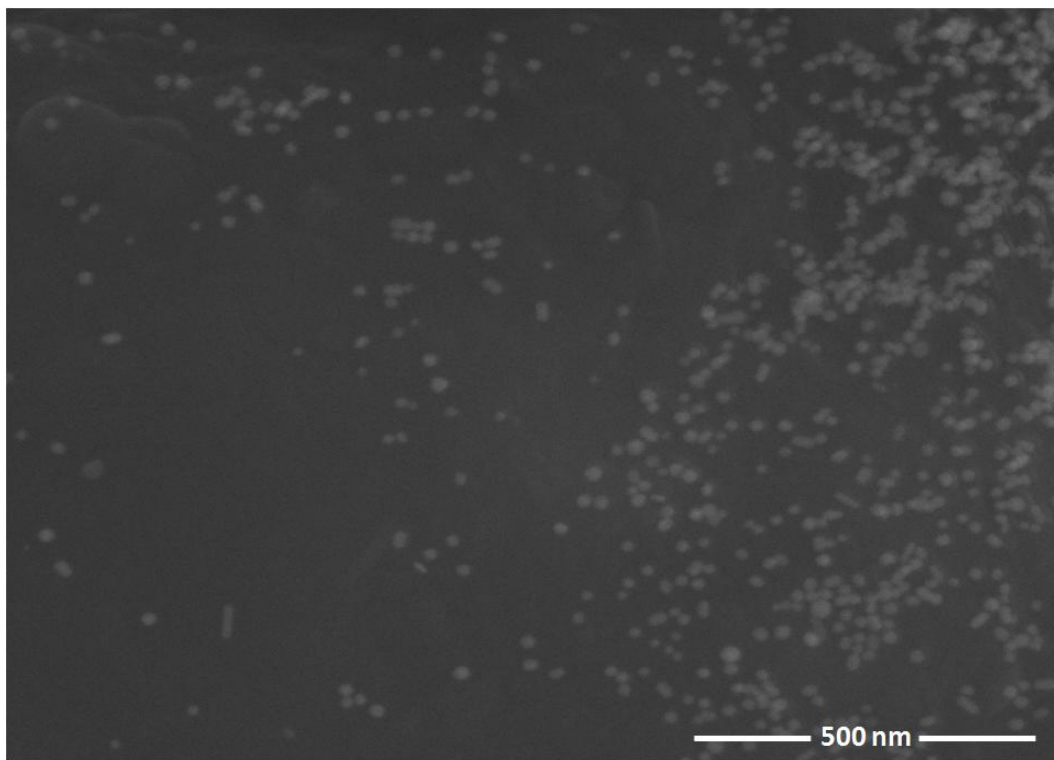


Figure 5.2. SEM images of seed particles attached on ITO surface.

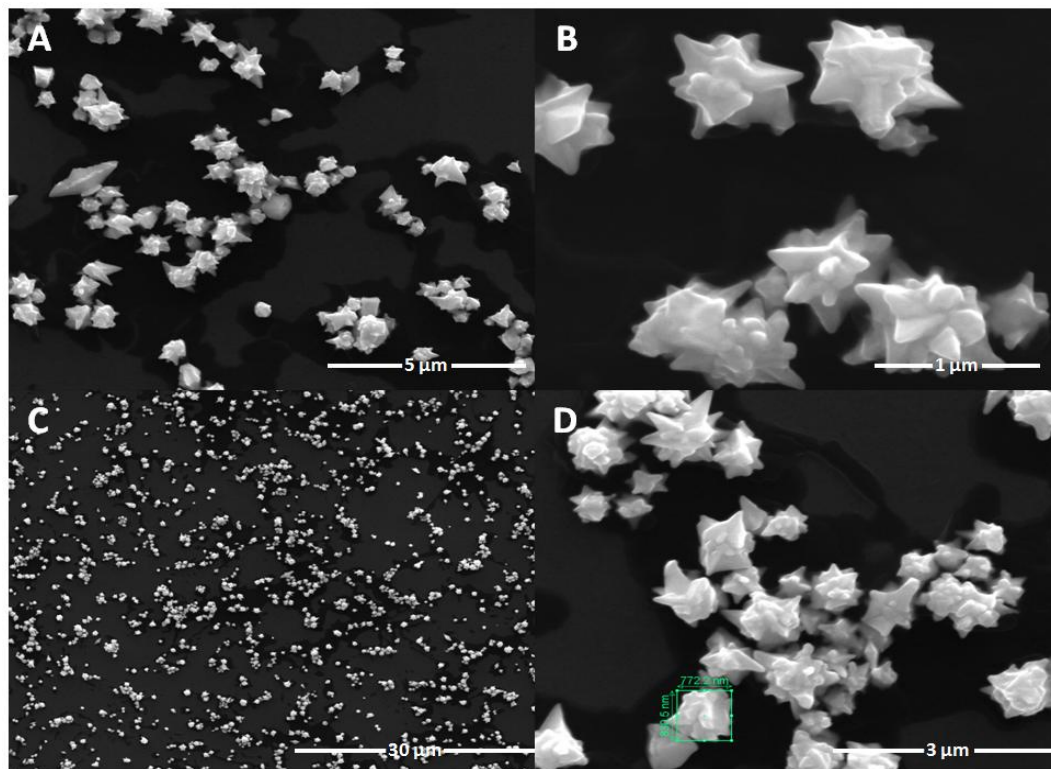


Figure 5.3. SEM images of the branched gold nanoparticles on ITO surface. ITO substrates were immersed in seed solution for 30 minutes. Figures from (a) to (d) show images at different magnifications.

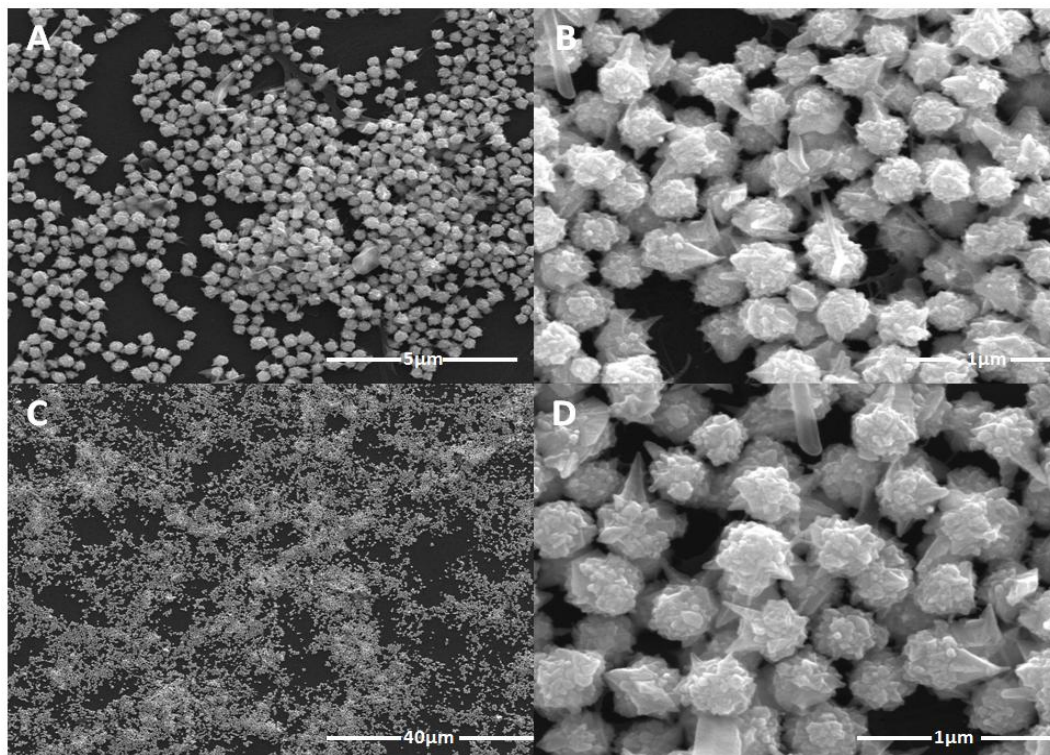


Figure 5.4. SEM images of the branched gold nanoparticles on glass surface. Glass substrates were immersed in seed solution for 30 minutes. Figure from A to D shows images at different magnifications.

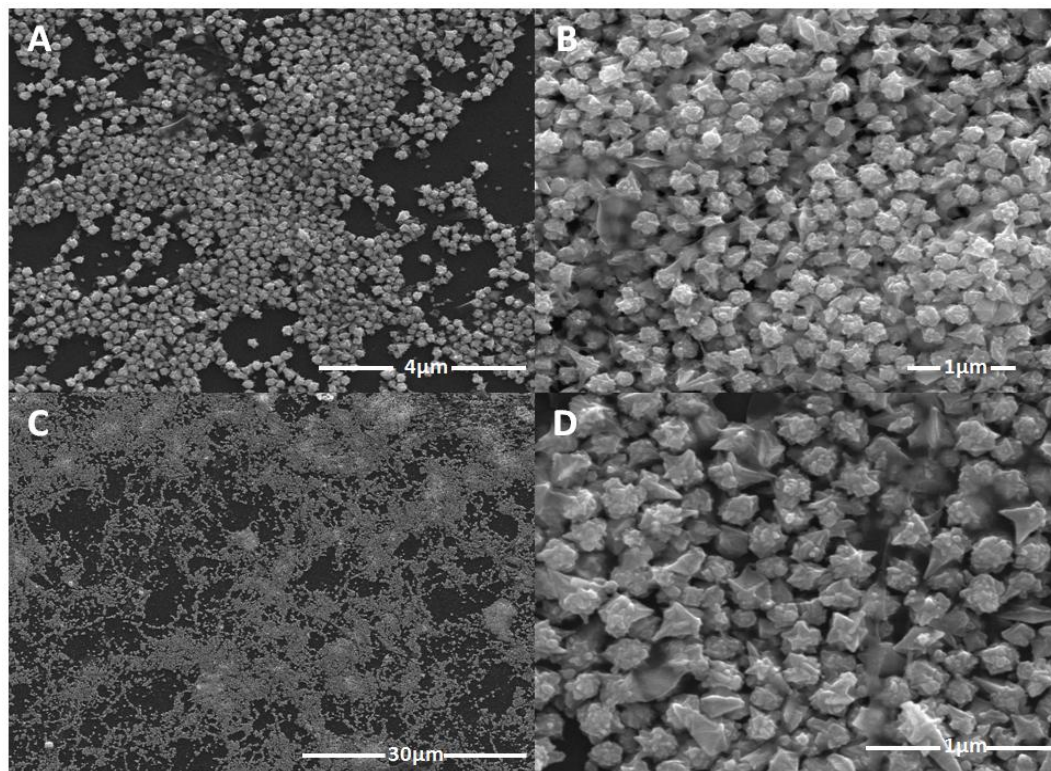


Figure 5.5. SEM images of the branched gold nanoparticles on Si surface. Glass substrates were immersed in seed solution for 30 minutes. Figures from (a) to (d) show images at different magnifications.

5.4. CONCLUSION

We succeeded in attaching branched gold nanoparticles onto the ITO surface by using seed-mediated growth method in the presence of APTMS and evaluate the results with SEM analysis. We studied the incubation times from 5 seconds to 60 minutes. According to the results of SEM analysis, there was no significant change in density of nanoparticles on the surfaces, suggesting very fast deposition of seed particles.

Nanoparticles have shown similar morphologies and size distribution when produced at different substrates. This means that substrate does not affect the morphologies of nanoparticles.

Purification steps do not cause a washing out of the branched gold nanoparticles from the surface indicating strong interactions between the substrate and the particles.

Density of nanoparticles on ITO surfaces is less as compared to Si and glass surface for the same incubation time. This is possibly because of less effective attachment of APTMS to the ITO surface as compared to Si and glass surfaces.

The applications of substrates with branched gold nanoparticles generated in the presence of APTMS are promising. They can be used, for instance, in optoelectronics as substrates of conjugated polymer-based organic solar cells. Applications of substrates with branched gold nanoparticles are now in progress.

REFERENCES

- [1] P. Photovoltaics, "A Practical Approach. Ed. FC Krebs," SPIE Press, Bellingham, Washington, 2008.
- [2] Y. Zhou, M. Eck, and M. Krüger, "Bulk-heterojunction hybrid solar cells based on colloidal nanocrystals and conjugated polymers," *Energy Environ. Sci.*, vol. 3, no. 12, pp. 1851-1864, 2010.
- [3] D. H. Wang *et al.*, "Enhancement of Donor–Acceptor Polymer Bulk Heterojunction Solar Cell Power Conversion Efficiencies by Addition of Au Nanoparticles," *Angewandte Chemie*, vol. 123, no. 24, pp. 5633-5637, 2011.
- [4] H. Bi, and R. LaPierre, "A GaAs nanowire/P3HT hybrid photovoltaic device," *Nanotechnology*, vol. 20, pp. 465205, 2009.
- [5] M. Hiramoto, G. Site, and H. Contacts, "Organic Solar Cells Incorporating ap–i–n Junction and ap–n Homojunction," 2005.
- [6] I. Uechi, and S. Yamada, "Photochemical and analytical applications of gold nanoparticles and nanorods utilizing surface plasmon resonance," *Analytical and bioanalytical chemistry*, vol. 391, no. 7, pp. 2411-2421, 2008.
- [7] S. Barbosa *et al.*, "Tuning size and sensing properties in colloidal gold nanostars," *Langmuir*, 2010.
- [8] P. Zijlstra *et al.*, "High-temperature seedless synthesis of gold nanorods," *The Journal of Physical Chemistry B*, vol. 110, no. 39, pp. 19315-19318, 2006.
- [9] A. Alekseeva *et al.*, "Gold nanorods: Synthesis and optical properties," *Colloid Journal*, vol. 68, no. 6, pp. 661-678, 2006.
- [10] F. Hao *et al.*, "Plasmon resonances of a gold nanostar," *Nano letters*, vol. 7, no. 3, pp. 729-732, 2007.
- [11] P. Senthil Kumar *et al.*, "High-yield synthesis and optical response of gold nanostars," *Nanotechnology*, vol. 19, pp. 015606, 2008.
- [12] E. Nalbant Esenturk, and A. Hight Walker, "Surface-enhanced Raman scattering spectroscopy via gold nanostars," *Journal of Raman Spectroscopy*, vol. 40, no. 1, pp. 86-91, 2009.
- [13] L. Rodríguez-Lorenzo *et al.*, "Surface Enhanced Raman Scattering Using Star-Shaped Gold Colloidal Nanoparticles†," *The Journal of Physical Chemistry C*, vol. 114, no. 16, pp. 7336-7340, 2009.
- [14] M. Kambayashi, J. Zhang, and M. Oyama, "Crystal growth of gold nanoparticles on indium tin oxides in the absence and presence of 3-mercaptopropyl-trimethoxysilane," *Crystal growth & design*, vol. 5, no. 1, pp. 81-84, 2005.
- [15] B. Bhushan, *Springer handbook of nanotechnology*: Springer Verlag, 2004.
- [16] J. F. Mongillo, *Nanotechnology 101*: Greenwood Pub Group, 2007.
- [17] R. W. Kelsall *et al.*, *Nanoscale science and technology*: Wiley Online Library, 2005.
- [18] M. R. Wiesner, and J.-Y. Bottero, *Environmental nanotechnology*: McGraw-Hill Professional, 2007.
- [19] T. Pradeep, *Nano The Essentials*: Tata McGraw-Hill, 2007.

- [20] J. M. Köhler, and W. Fritzsche, *Nanotechnology: an introduction to nanostructuring techniques*: Vch Verlagsgesellschaft Mbh, 2007.
- [21] H. Gleiter, "Nanostructured materials: basic concepts and microstructure," *Acta materialia*, vol. 48, no. 1, pp. 1-29, 2000.
- [22] N. M. S. Cameron, and M. E. Mitchell, *Nanoscale: issues and perspectives for the nano century*: Wiley-interscience, 2007.
- [23] H. HANNINK, and A. Hill, "Nanostructure control of materials," *Recherche*, vol. 67, pp. 02, 2006.
- [24] L. D. GAsMAN, "Nanotechnology applications & market," *Recherche*, vol. 67, pp. 02, 2006.
- [25] R. Siegel, A. Edelstein, and R. Cammarata, "Nanomaterials: synthesis, properties and applications," *Edited by: Edelstein, AS and Cammarata, RC*, vol. 207, pp. 243-245, 1996.
- [26] C. Saw, "X-ray Scattering Techniques for Characterization Tools in the Life Sciences, Nanotechnologies for the Life Science, edited by Challa Kumar," Wiley-VCH Verlag GmbH and Company, KGaA, Weinheim, 2006.
- [27] E. Y. Vedmedenko, *Competing interactions and patterns in nanoworld*: Vch Verlagsgesellschaft Mbh, 2007.
- [28] U. Guler, and R. Turan, "Effect of particle properties and light polarization on the plasmonic resonances in metallic nanoparticles," *Optics Express*, vol. 18, no. 16, pp. 17322-17338, 2010.
- [29] K. J. Klabunde, R. Richards, and MyiLibrary, *Nanoscale materials in chemistry*: Wiley Online Library, 2001.
- [30] C. J. Murphy *et al.*, "Anisotropic metal nanoparticles: synthesis, assembly, and optical applications," *The Journal of Physical Chemistry B*, vol. 109, no. 29, pp. 13857-13870, 2005.
- [31] M. J. A. Hore, and R. J. Composto, "Nanorod Self-Assembly for Tuning Optical Absorption," *ACS nano*, 2010.
- [32] S. E. Shaheen, D. S. Ginley, and G. E. Jabbour, "Organic-based photovoltaics: toward low-cost power generation," *MRS bulletin*, vol. 30, no. 01, pp. 10-19, 2005.
- [33] A. Goetzberger, and V. U. Hoffmann, *Photovoltaic solar energy generation*: Springer Verlag, 2005.
- [34] G. Cao, and C. J. Brinker, *Annual review of nano research*: World Scientific Pub Co Inc, 2006.
- [35] S. S. Sun, and N. S. Sariciftci, *Organic photovoltaics: mechanism, materials, and devices*: CRC, 2005.
- [36] G. P. Smestad, *Optoelectronics of solar cells*: Society of Photo Optical, 2002.
- [37] T. Sōga, *Nanostructured materials for solar energy conversion*: Elsevier Science, 2006.
- [38] C. Tang, "Two-layer organic photovoltaic cell," *Applied Physics Letters*, vol. 48, no. 2, pp. 183-185, 1986.
- [39] Y. Liang *et al.*, "For the bright future—bulk heterojunction polymer solar cells with power conversion efficiency of 7.4%," *Advanced Materials*, vol. 22, no. 20, pp. E135-E138, 2010.

- [40] S. Ren *et al.*, "Heterojunction photovoltaics using GaAs nanowires and conjugated polymers," *Nano letters*, 2011.
- [41] L. Tsakalakos, "Nanostructures for photovoltaics," *Materials Science and Engineering: R: Reports*, vol. 62, no. 6, pp. 175-189, 2008.
- [42] J. R. Maiolo III *et al.*, "High aspect ratio silicon wire array photoelectrochemical cells," *Journal of the American Chemical Society*, vol. 129, no. 41, pp. 12346-12347, 2007.
- [43] L. Hu, and G. Chen, "Analysis of optical absorption in silicon nanowire arrays for photovoltaic applications," *Nano letters*, vol. 7, no. 11, pp. 3249-3252, 2007.
- [44] O. L. Muskens *et al.*, "Design of light scattering in nanowire materials for photovoltaic applications," *Nano letters*, vol. 8, no. 9, pp. 2638-2642, 2008.
- [45] D. C. Olson *et al.*, "Effect of polymer processing on the performance of poly (3-hexylthiophene)/ZnO nanorod photovoltaic devices," *The Journal of Physical Chemistry C*, vol. 111, no. 44, pp. 16640-16645, 2007.
- [46] D. D. S. Fung *et al.*, "Optical and electrical properties of efficiency enhanced polymer solar cells with Au nanoparticles in a PEDOT-PSS layer," *J. Mater. Chem.*, vol. 21, no. 41, pp. 16349-16356, 2011.
- [47] C. C. D. Wang *et al.*, "Optical and electrical effects of gold nanoparticles in the active layer of polymer solar cells," *J. Mater. Chem.*, vol. 22, no. 3, pp. 1206-1211, 2011.
- [48] Z. G. Li *et al.*, "Organic thin-film solar cells: Devices and materials," *SCIENCE CHINA Chemistry*, pp. 1-25, 2012.
- [49] S. Günes, H. Neugebauer, and N. S. Sariciftci, "Conjugated polymer-based organic solar cells," *Chemical Reviews*, vol. 107, no. 4, pp. 1324-1338, 2007.
- [50] R. Po *et al.*, "Polymer-and carbon-based electrodes for polymer solar cells: Toward low-cost, continuous fabrication over large area," *Solar Energy Materials and Solar Cells*, 2012.
- [51] M. D. Archer, and A. J. Nozik, *Nanostructured and photoelectrochemical systems for solar photon conversion*: Imperial College Pr, 2008.
- [52] R. Po, M. Maggini, and N. Camaioni, "Polymer solar cells: recent approaches and achievements," *The Journal of Physical Chemistry C*, vol. 114, no. 2, pp. 695-706, 2009.
- [53] M. Di Ventra, S. Evoy, and J. R. Heflin, *Introduction to nanoscale science and technology*: Springer, 2004.
- [54] G. Yu *et al.*, "Polymer photovoltaic cells: enhanced efficiencies via a network of internal donor-acceptor heterojunctions," *Science*, vol. 270, no. 5243, pp. 1789-1791, 1995.
- [55] C. Brabec *et al.*, "Organic photovoltaic devices produced from conjugated polymer/methanofullerene bulk heterojunctions," *Synthetic metals*, vol. 121, pp. 1517-1520, 2001.
- [56] J. Xiao, and L. Qi, "Surfactant-assisted, shape-controlled synthesis of gold nanocrystals," *Nanoscale*, vol. 3, no. 4, pp. 1383-1396, 2011.
- [57] H. A. Atwater, and A. Polman, "Plasmonics for improved photovoltaic devices," *Nature materials*, vol. 9, no. 3, pp. 205-213, 2010.

- [58] W. Sha, W. Choy, and W. Chew, "A comprehensive study for the plasmonic thin-film solar," *Optics Express*, vol. 18, no. 6, pp. 5993-6007, 2010.
- [59] X. Jiang, A. Brioude, and M. Pileni, "Gold nanorods: Limitations on their synthesis and optical properties," *Colloids and Surfaces A: Physicochemical and Engineering Aspects*, vol. 277, no. 1, pp. 201-206, 2006.
- [60] L. Qiao *et al.*, "Localized surface plasmon resonance enhanced organic solar cell with gold nanospheres," *Applied Energy*, vol. 88, no. 3, pp. 848-852, 2011.
- [61] J. Xie *et al.*, "The synthesis of SERS-active gold nanoflower tags for in vivo applications," *ACS nano*, vol. 2, no. 12, pp. 2473-2480, 2008.
- [62] T. K. Sau, and C. J. Murphy, "Room temperature, high-yield synthesis of multiple shapes of gold nanoparticles in aqueous solution," *Journal of the American Chemical Society*, vol. 126, no. 28, pp. 8648-8649, 2004.
- [63] N. R. Jana, L. Gearheart, and C. Murphy, "Seed-mediated growth approach for shape-controlled synthesis of spheroidal and rod-like gold nanoparticles using a surfactant template," *Advanced Materials*, vol. 13, no. 18, pp. 1389-1393, 2001.
- [64] N. Taub, O. Krichevski, and G. Markovich, "Growth of gold nanorods on surfaces," *The Journal of Physical Chemistry B*, vol. 107, no. 42, pp. 11579-11582, 2003.
- [65] A. Gole, and C. J. Murphy, "Seed-mediated synthesis of gold nanorods: role of the size and nature of the seed," *Chemistry of Materials*, vol. 16, no. 19, pp. 3633-3640, 2004.
- [66] X. Kou *et al.*, "Curvature-directed assembly of gold nanocubes, nanobranches, and nanospheres," *Langmuir*, vol. 25, no. 3, pp. 1692-1698, 2008.